Elastic Electron Scattering in Gases

J. HOWARD MCMILLEN
Kansas State College, Manhattan, Kansas

1. INTRODUCTION

THIS report is a discussion of a group of researches that began to appear in the scientific literature around 1927 and which dealt with elastic collisions between electrons and gaseous molecules. In these researches a well-defined beam of electrons was allowed to penetrate a gas-filled chamber and the number of electrons scattered from the beam at various scattering angles was measured. The original investigators in the field hoped, no doubt, to accomplish two things by this type of experiment. They hoped not only to enhance the existing knowledge of atomic structure but also to determine the behavior of an electron beam when the beam was scattered by an atom whose dimensions were comparable with the beam's associated de Broglie wave-length. With regard to investigating atomic structure, it has been pointed out that the electron more or less plays the role of a probe; the atom's electrostatic field is the region to be probed. This conception of the electron as a probe probably seems more plausible to the experimenter since he can by proper regulation of the electron's energy choose that part of the atom he wishes to probe. For example, if he wishes to explore the L and M shells of an atom like argon, he uses electrons with energies somewhere near 50 electron volts. To investigate the region nearer the nucleus he employs faster electrons, electrons whose energies are to be measured in kilovolts. The experimental data yielded by these investigations have in almost all cases given evidence that the atomic fields are those predicted by the best available method of wave mechanics. Besides this rather important confirming evidence regarding atomic structure, these researches have also shown that the classical particle theory of an atom-electron collision is wholly inadequate, except when the electrons are moving with very large velocities. The wave theory,[1] on the other hand, has been so successful in its interpretation of these scattering experiments that these experiments may now be regarded as important experimental evidence supporting the wave theory of electron propagation.

2. SCATTERING OF ELECTRONS AS PARTICLES

The conception of the electron as a probe is of course only acceptable if the electron beam is considered to be composed of electron particles rather than a beam of de Broglie electron waves. In the scattering process, according to the classical particle theory, the colliding electron describes within the atom a curved path, as it is attracted towards the center of the atom by some sort of centralized electrostatic force. The angle of scattering θ is defined as the angle between the radial path of departure from the atom and the electron's initial direction. The magnitude of this angle depends upon the kind of field through which the electron passes, upon how fast the electron was initially moving, and just how it was approaching the scattering atom. The latter factor is represented by the impact parameter p which is defined as the shortest distance between the center of the atom and the electron's path had the electron passed on without being deflected. Since all manners of approach are possible, which is equivalent to saying that all values of p are equally probable, the problem is solved as soon as the relationship between θ and p is found. From this relationship the number of paths leaving the atom between the angles θ and $\theta+d\theta$ can be easily ascertained. It is thus apparent that the problem of particle scattering is that of finding the distribution of electron paths within the scattering atom. It has been shown that if the atomic force field is an inverse-square-law field, that is, the field that would accompany a bare nucleus, the paths are hyperbolas with the scattering center at one of the foci. The relationship between scattering

angle and impact parameter for this field is given by

$$\tan \theta/2 = 2Ze^2/Ep, \qquad (1)$$

where Ze is the nuclear charge and E the initial kinetic energy of the electron. Fig. 1 shows several of these paths for particles undergoing a deflection in the field of a bare nucleus. With all manners of the electron's approach equally probable, this field gives a preponderance of paths in the forward direction. The majority of electrons show very little deviation in their passage through a field furnished by a bare nucleus and the scattering curve follows a cosec^4 $(\theta/2)$ law.

One becomes aware of the fact that in the particle theory the position of each individual electron is known throughout the scattering process. Every scattered electron has one direction of approach or impact parameter p, and follows a specific path through the scattering field. For example, one can say of every 500-volt electron which has been scattered at an angle $\theta = 120°$ by a bare hydrogen nucleus, that it has approached the nucleus as if to pass it at a distance of 0.033 angstrom and has followed a a hyperbolic orbit coming as close as 0.013 angstrom to the nucleus at the apex of its orbit.

The expression for the number of electrons scattered per unit solid angle at the angle θ, when the central force field varies as Ze^2/r^2, is given by

$$I(\theta) = (Z^2e^4 \text{ cosec}^4 (\theta/2))/16E^2. \qquad (2)$$

The above expression was first developed by Rutherford for the scattering of α-particles by an atomic nucleus. For any other type of central field the path may be determined[2] from the relationship

$$I(\theta) = (J/m^2v^2 \sin \theta)(dJ/d\theta)$$

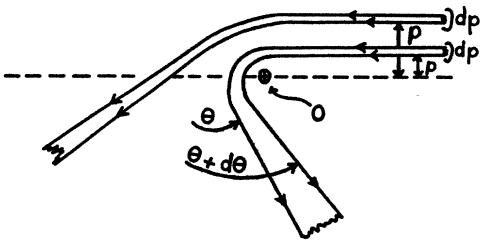

FIG. 1. Schematic diagram of several electron paths in the Coulomb field surrounding a bare nucleus located at O.

in which J may be found from

$$\theta/2 - \pi/2 - \int_{r_0}^{\infty} (\partial/\partial J)\,(2m(E-V) - J^2/r^2)^{\frac{1}{2}} dr = 0,$$

where r_0 is the positive zero of the term in the brackets. The quantity V in the expression is the potential field. Only the inverse-square-law field, however, leads to a simple analytical expression such as (2) for the scattering formula.

3. Scattering of Electron Waves

In the wave theory of scattering the beam of electrons which is directed into the scattering chamber is represented by a plane wave of wavelength $\lambda = h/mv$. In the scattering experiments discussed here the electron energies range, for the most part, from one to a thousand electron volts and thus the associated de Broglie wavelengths vary from about one-half angstrom to ten angstroms. The very fact that these wavelengths are comparable with atomic dimensions suggests that the explanations of the scattering events involve a diffraction phenomenon. It develops that this suggestion is correct and as a result the scattering theories lead to solutions of two general types. One of these resembles Raleigh's treatment of the scattering of sound waves by small particles and the Mie-Debye theory of the scattering of light waves by small spheres. The other is an application of Huygens' principle as it has been applied to the scattering of light.

To understand the conditions under which these two theories are applicable one first defines atomic "size" as it is used in the theory of electron-atom collisions. Here "size" depends not only upon the extent of the atomic field but also upon the energy of the colliding electron. "Size" is defined as that radial distance r_c at which the potential field of the atom numerically equals the electron's initial kinetic energy. The effective size, or r_c, is thus flexible, diminishing as faster colliding electrons are considered.

It has been found that the ratio of the colliding electron's wave-length λ_0 to the effective atomic radius r_c may be used as a criterion for designating just when these two types of wave theories are best applied. It can be shown that if λ_0/r_c is

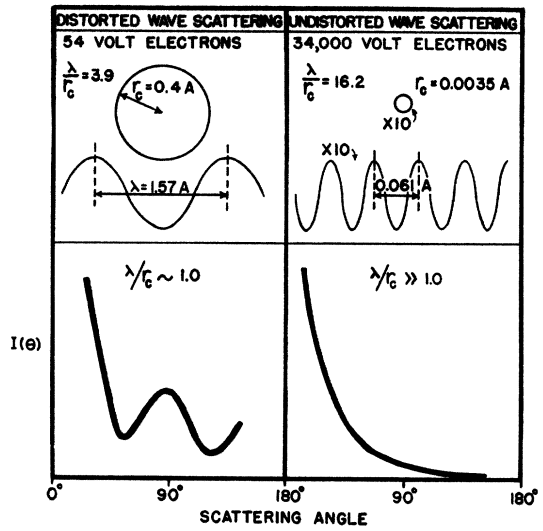

FIG. 2. Scattering curves of argon representing distorted and undistorted wave scattering. Corresponding ratios of wave-lengths to argon atomic radii, r_c, also shown.

about unity, the amplitude of the wave representing the plane incident beam is practically unaltered as it passes through the scattering atom. This is equivalent to representing the incident wave everywhere throughout the atomic field by the plane wave expression exp (ikz). If, however, $\lambda_0 \gg r_c$ this approximation is no longer plausible and the incident wave front becomes appreciably distorted inside the scattering atom. It has become customary to describe the scattering associated with these two theoretical treatments as the scattering of distorted and undistorted waves. Cases of scattering occurring with distortion are easily distinguished from those without by the nature of the scattering curves. Scattering curves from distorted wave scattering show peaks and valleys suggestive of diffraction patterns, whereas the undistorted wave scattering gives curves which fall off monotonically with angle.

The theories using Huygens' principle lend themselves best to the treatment of those cases in which the wave fronts are distorted only a little as the wave passes through the atom. That is to say, Huygens' method is used most successfully when the electron's associated de Broglie wave-length is of the same order of magnitude as the effective atomic radius r_c. When, however, $\lambda_0 \gg r_c$, a method patterned after the optical Mie-Debye method is more advantageously used. In Fig. 2 are shown two scattering curves for argon which are representative of these two types of wave scattering. The curves are accompanied by a diagram showing the relative magnitudes of the effective radius r_c, and the wave-length of the scattered wave. The calculations for Fig. 2 were made by using the Thomas-Fermi values for the field. One observes that fast electron scattering is of the undistorted wave type whereas the slow electron scattering is of the distorted wave type.

4. Wave Scattering with Distortion

The Mie-Debye wave problem of scattering is simply that of finding the amplitude of the wave ψ at large radial distances from the scattering atom, where ψ for this particular problem is a solution of Schrodinger's wave equation. The incident beam is represented by a plane wave of unit amplitude traveling in the z direction

$$\psi_i = \exp(ikz). \tag{3}$$

The scattered wave ψ_s travels out radially from the scattering atom with an amplitude which is a function of θ as well as r. In this expression

$$k = 2\pi/\lambda = mv2\pi/h = 2^{\frac{1}{2}}E^{\frac{1}{2}}m^{\frac{1}{2}}\pi/h \tag{4}$$

in which λ is the associated de Broglie wave-length. The sum of these two waves

$$\psi(r, \theta) = \psi_i + \psi_s$$

is a solution of Schrödinger's equation

$$\nabla^2\psi + (k^2 - 8\pi^2 m V(r)/h^2)\psi = 0 \tag{5}$$

in which $V(r)$ is the spherically symmetrical potential field of the scattering atom. Schrodinger's equation as it stands is difficult to solve directly, partly because the atomic field $V(r)$ cannot be expressed as a simple function of r. However, a solution of Eq. (5), which is valid, incidentally, for distorted as well as undistorted waves, has been obtained by Faxen and Holtsmark[3] by means of an expansion of the ψ's.

In the Faxen and Holtsmark solution ψ is expanded into a series of smaller amplitude terms.[4] In applying this expansion it is convenient to apply it first to the incident wave.

Let $\psi_i(r, \theta)$ be divided into a θ and an r function, thus

$$\psi_i(r, \theta) = \Theta(\theta)g(r)/r. \quad (6)$$

Schrödinger's equation for only the incident wave is obtained by setting $V(r)=0$ in (5), which gives

$$\nabla^2\psi_i + k^2\psi_i = 0. \quad (7)$$

A well-known solution to this equation is

$$\psi_i(r, \theta) = C_i \sum_{n=0}^{n=\infty} P_n(\cos\theta)g_n(r)/r, \quad (8)$$

where the g_n's are solutions of the following series of differential equations

$$d^2g_n/dr^2 + (k^2 - n(n+1)/r^2)g_n = 0. \quad (9)$$

The n's appear originally in the solution as whole number indices but further considerations show that they also have a physical significance. They are the angular momentum quantum numbers associated with the electrons in the incident beam. So one observes that the incident electron wave has been expanded into a series of terms in which each term is associated with a different angular momentum quantum number n. Each term also shows a different angular distribution which is given by the Legendre coefficients $P_n(\cos\theta)$. These individual terms in the expansion of ψ_i play a role similar to the various impact parameters p belonging to the individual electrons of the beam in the particle theory. A similar treatment carried out for the scattered wave gives with the aid of (5),

$$\psi_s(r, \theta) = C_s \sum_{n=0}^{n=\infty} P_n(\cos\theta)G_n(r)/r \quad (10)$$

in which the G_n's are solutions of

$$d^2G_n/dr + (k^2 - 8\pi^2 m V(r)/h^2 - n(n+1)/r^2)G = 0. \quad (11)$$

Although a solution of (11) with the proper boundary condition yields at once the amplitude distribution of the scattered wave this solution is not required, since one is interested in ψ_s only at large distances from the scattering center. Thus one is able to postpone the difficult task of determining ψ within the atomic field by obtaining only asymptotic solutions of (9) and (11). The asymptotic solution of (9) for the incident wave gives the sinusoidal expression

$$\psi_i(\theta, r \doteq \infty) = C_i \sum_{n=0}^{n=\infty} P_n(\cos\theta) \times \sin(kr - n\pi/2)/kr = \exp(ikz). \quad (12)$$

One notes that the asymptotic solution for the scattered wave should have the same general form as that of the incident wave, since (9) and (11) are identical for large r. The scattered wave differs from a plane wave solution only in the value of an arbitrary constant. This constant is the very significant phase shift constant η_n. The asymptotic solution of (11) for the scattered wave with the phase shift constant η_n introduced is

$$\psi_s(\theta, r \doteq \infty) = C_i \sum_{n=0}^{n=\infty} P_n(\cos\theta) \times \sin(kr - n\pi/2) + \eta_n)/kr. \quad (13)$$

Both $g(r)$ and $G(r)$ are zero at the origin, and sinusoidal but out of phase at large r and z. The behavior of $G_0(r)$ and $g_0(r)$ in going from the inside to the outside region of a scattering atom is shown in Fig. 3. The dotted lines in the figure depict $g_0(r)$, for the incident waves, and the solid lines $G_0(r)$ for the scattered wave in the region of the atomic scattering field. It is observed that the shift in phase is largest for slow electrons. These curves were computed by McDougall[5] for helium, using Hartree's values for the field. It is this phase shift which is largely

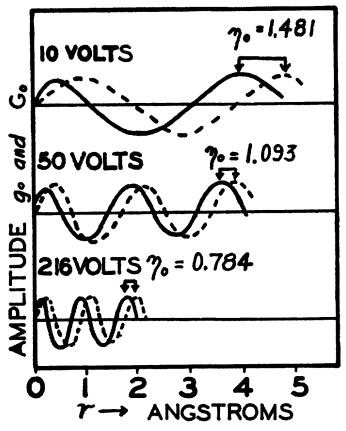

FIG. 3. Dotted lines represent $g_0(r)$ for incident wave and solid lines $G_0(r)$ for scattered wave in helium. Phase shifts η_0 are also indicated, arbitrary ordinate scale. McDougall, reference 5.

responsible for the ultimate shape of the scattering curve.

By satisfying the boundary conditions the constants C_1 and C_2 are also determined and the complete expression for the amplitude of the scattered wave becomes

$$\psi_s(\theta, r \doteq \infty) = (2ik)^{-1} \sum_{n=0}^{n=\infty} (2n+1) \times (\exp(2i\eta_n) - 1) \times P_n(\cos\theta) \exp(ikr)/r. \quad (14)$$

The number of electrons scattered per unit solid angle is given by the square of this amplitude and is

$$I(\theta) = A^2 + B^2,$$

where

$$A = (2k)^{-1} \sum_{n=0}^{n=\infty} (2n+1)(\cos 2\eta_n - 1) P_n(\cos\theta),$$
$$B = (2k)^{-1} \sum_{n=0}^{n=\infty} (2n+1) \sin 2\eta_n P_n(\cos\theta). \quad (15)$$

5. The Phase Shift

Although it is clear from the preceding section how η is introduced into the solution for the scattered wave, it is yet to be shown how it is related to the potential field $V(r)$. True, it can be obtained from direct numerical integration of the equation for $G(r)$ (11), but this is mathematically difficult. There are several approximate methods of calculating the η's from a given potential distribution $V(r)$, and perhaps the Wentzel-Kramers-Brillouin-Jeffreys method[6] is the most instructive. If the factor in the brackets of Eq. (11) were not a function of r, the solution of (11) would simply be $\exp(2\pi i K r)$ where K^2 is defined as the factor contained in the brackets. The W-K-B-J method makes use of the fact that if K varies very little while r is changing by not more than one wave-length, K can be replaced by an expression which takes on an aspect of an average value for K. Thus the W-K-B-J solution for the phase of the field wave is

$$\exp\left(2\pi i \int_{r=R_0}^{r=r} K dr\right). \quad (16)$$

The value of $r = R_0$ is that value of r at which K is equal to zero. By applying a similar approximation to the field-free wave and subtracting the two, we obtain for the phase shift, or the phase difference, η_n,

$$\eta_n = \int_{R_1}^{\infty} (k^2 + 8\pi^2 m V(r)/h^2 - n(n+1)/r^2)^{\frac{1}{2}} dr - \int_{R_2}^{\infty} (k^2 - n(n+1)/r^2)^{\frac{1}{2}} dr \quad (17)$$

or

$$\eta_n = \int_{R_1}^{\infty} K_s dr - \int_{R_2}^{\infty} K_u dr \quad (18)$$

in which R_1 and R_2 are the values of r for which K_s and K_u are zero. Generally the phase shifts are larger the larger the atomic field. They are also larger for slower electrons, that is, for electron beams of long wave-length. How these factors contribute to the numerical value of the phase shift may be seen in the schematic representations of Fig. 4 and Fig. 5. The shaded area in Fig. 5 is proportional to the phase shift.

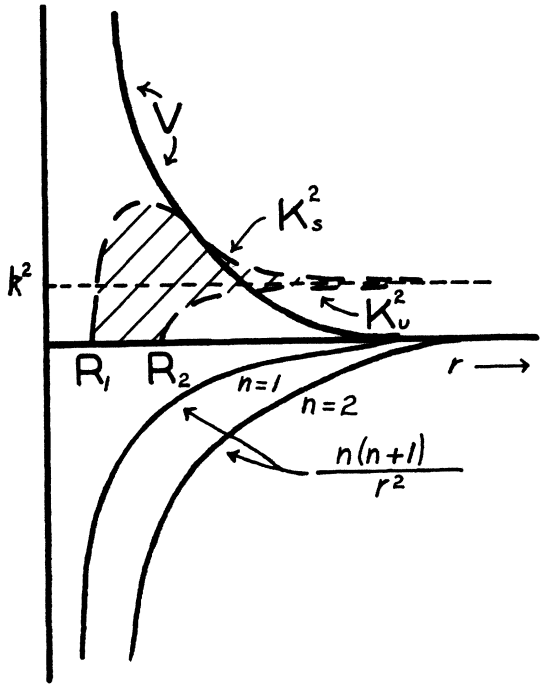

FIG. 4. Schematic diagram showing how the factors which affect the phase shift in Eq. (17) vary with r.

While the W-K-B-J method is excellent for visualizing how the phase shift is affected by k, V and n, it still gives only approximate values.

Just how accurate these values are will be discussed in Section 17 where they will be compared with other methods of arriving at phase shift data.

6. Amplitude Harmonics

From expression (14) giving the amplitude of the scattered wave, it is apparent that the amplitude is the sum of a series of individual terms. These are called harmonics. Each amplitude harmonic represents a wavelet with its own particular angular distribution. Thus, a beam of electrons having only electrons with $n=4$, if such a beam can be imagined, would yield a scattered wave given by P_4^2 (cos θ), that with $n=2$, P_2^2 (cos θ). These hypothetical distributions are shown in Fig. 6. It is a feature of the wave theory method that every harmonic contributes to the distribution of scattered electrons over the entire angular range. This is in direct contrast with the particle situation, where one impact parameter value accounts for electrons scattered at only one scattering angle. Since the amplitudes of these harmonics may have plus and minus values, one can speak of the intensity of the scattered wave as resulting from the interference effect of the various harmonics. As to the magnitude of each harmonic, we see that it depends upon n and the atomic field $V(r)$. These factors are contained in $(2n+1)$ and $(\exp(2i\eta_n)-1)$, respectively. It develops that frequently the latter expression is zero for all but one or two harmonics, so that the shape of the scattering curve may depend upon only a few Legendre coefficients. In fact, there are many examples where the scattering curves take on the form given by the squares of just one Legendre coefficient.

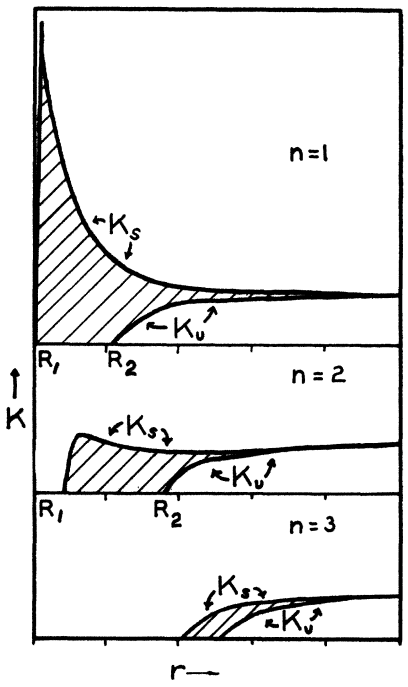

Fig. 5. The areas under the curves are proportional to the phase shifts, growing smaller for larger angular momentum quantum numbers n. Schematic diagram.

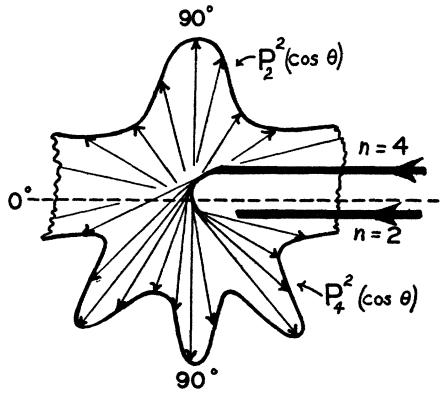

Fig. 6. Hypothetical distribution of scattered electrons realized for harmonics $n=2$ and $n=4$.

Since the n's are the angular momentum quantum numbers, each harmonic is identified with a physical property of the particle electron. The n's are analogous to the impact parameters p of the particle theory, since they give the approximate distances at which the electrons would pass the scattering center were they to pass on undeflected. The harmonics of small n, for example, refer to the electrons of small angular momentum which pass near the nucleus whereas those of very large n correspond to those which might even be so far removed as to be undeflected by the atomic field. If n equals 2π times the angular momentum, then with the aid of the defining equation (4) for k it can be shown that n is related to p by the expression

$$p=n/k=n\lambda/2\pi=1.94n/(\text{electron volts})^{\frac{1}{2}}, \quad (19)$$

where p in the last term is expressed in angstrom units.

7. Wave Scattering Without Distortion

In the preceding treatment of the wave problem the scattered wave was treated as if it were the vector sum of a series of harmonics. Born's treatment of the problem leads to an entirely different mathematical form for the amplitude of the scattered wave and suggests a different picture of the scattering process. According to Born's theory, when the plane wave strikes the atom each volume element in the atom sends out a spherical wavelet. These wavelets start out in phase but possess different amplitudes depending upon the value of the potential field at the volume element. The resultant amplitude of the scattered wave is then obtained by summing vectorially all the amplitudes of the individual wavelets. This is identical with the optical method of Huygens and Kirchhoff.

In Born's treatment[7] use was made of the fact that Schrodinger's wave equation (5) when written in the form

$$\nabla^2\psi+k^2\psi=8\pi^2mh^{-2}V(r')\psi(r') \qquad (20)$$

has a solution[8]

$$\psi=\psi_i(x,y,z)-\frac{2\pi m}{h^2}\int\frac{\exp\,(ik|\mathbf{r}-\mathbf{r}'|)}{|\mathbf{r}-\mathbf{r}'|}\times V(r')\psi(r')d\tau', \qquad (21)$$

where ψ_i is a solution of

$$\nabla^2\psi_i+k^2\psi_i=0$$

or is simply the incident wave, $\psi_i=\exp\,(ikz)$. In expression (21) the primes refer to the coordinates of the atom. The bold face symbols are vectors. It can be easily shown that for large values of r (21) becomes

$$\psi=\exp\,(ikz)-2\pi mr^{-1}h^{-2}\exp\,(ikr)\times\int_0^\infty\exp\,(-ik\mathbf{n}\cdot\mathbf{r}')V(r')\psi(\mathbf{r}')d\tau', \qquad (22)$$

where $\mathbf{n}$ is a unit vector in the direction of r. Since in the above expression (22) $\psi(\mathbf{r}')$ is not known, Born proposed that an approximate form for $\psi(\mathbf{r}')$ be adopted. Born replaced $\psi(\mathbf{r}')$ by $\exp\,(ikz')$ which is simply the expression for an undistorted incident wave. Born's approximation amounted to assuming that the amplitude of the incident wave remains undistorted in its passage through the atom.

We now define the scattering function $f(\theta)$ by

$$\psi=\psi_i+\psi_s=\exp\,(ikz)-r^{-1}f(\theta)\exp\,(ikr) \qquad (23)$$

and by comparison with (22), write

$$f(\theta)=-\int\exp\,(ik(\mathbf{n}_0-\mathbf{n})\cdot r)2\pi mh^{-2}V(r)d\tau, \qquad (24)$$

where $\mathbf{n}_0$ is unit vector along the z axis so that $z=\mathbf{n}_0\cdot\mathbf{r}$.

From the form of expression (24) it is apparent that the scattered wave is that which would be produced if each volume element was the origin of a wavelet with an amplitude equal to $2\pi mV(r)/h^2$. The integral (24) may be partially integrated in the spherical polar form to give

$$f(\theta)=-8\pi^2mh^{-2}\int_0^\infty\frac{\sin\,(4\pi\mu r)V(r)}{4\pi\mu r}r^2dr \qquad (25)$$

in which μ stands for $\lambda^{-1}\sin\,(\theta/2)$. Born's formula (25) gives a smooth scattering curve which falls off monotonically with angle. The amplitude of the scattered wave is greater at small angles, as is evident from an inspection of Fig. 7 which illustrates formula (25). The scattered curve $f^2(\theta)$ can be obtained at once from (25) by a series of integrations whenever the data for the field $V(r)$ are available.

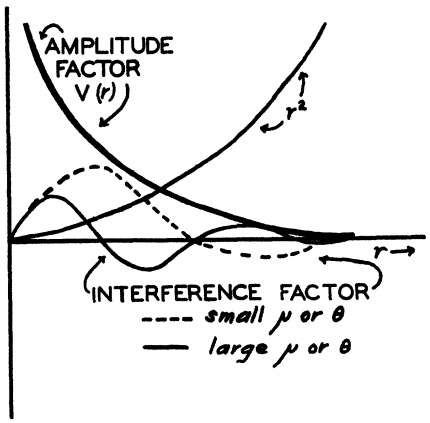

Fig. 7. An illustration of the behavior of those quantities which affect the amplitude of the scattered electron wave as given in Eq. (25).

8. X-Ray Structure Factors and Electron Scattering

Mott[9] greatly simplified the above expression by introducing the atomic structure factor F defined by

$$F(\mu)=4\pi\int_0^\infty \rho(r)\frac{\sin 4\pi\mu r}{4\pi\mu r}r^2dr, \qquad (26)$$

where $-e\rho(r)$ is the charge density. When $V(r)$ in (25) is replaced by

$$V(r)=-\frac{Ze^2}{r}+e^2\int\frac{\rho(r')d\tau'}{|\mathbf{r}-\mathbf{r}'|} \qquad (27)$$

and use is made of (26) we have

$$f(\theta)=\frac{e^2}{2mv^2}(Z-F(\mu))\ \mathrm{cosec}^2\ (\theta/2). \qquad (28)$$

This may also be written

$$f(\theta)=\frac{me^2Z}{2h^2\mu^2}-\frac{me^2F(\mu)}{2h^2\mu^2}. \qquad (29)$$

The first term of (29) is the scattered amplitude to be expected from the nucleus if it were devoid of atomic electrons while the second is the amplitude to be expected from the atomic electrons if they were all located at the center of the atom and had the effective charge $F(\mu)$. We infer from this that the amplitude of the scattered wave is the sum of a nuclear wave and a negative atomic electron wave in which both waves are scattered according to the inverse-square law and in which the central charges are Z and F, respectively.

It is convenient to write the intensity of the scattered wave as

$$I(\theta)=f^2(\theta)=\frac{m^2e^4Z^2}{4h^4\mu^4}\left(1-\frac{2F(\mu)}{Z}+\frac{F^2(\mu)}{Z^2}\right). \qquad (30)$$

The behavior of $f(\theta)$ as μ varies is shown in Fig. 8 where the ratio of the nuclear and electronic scattering to the scattering of a bare nucleus are plotted against μ. One observes that since F is a function of θ that, unlike bare nuclear scattering, the atomic scattering curve varies in shape for different electron energies and different atoms. The curves of Fig. 8 reveal how at large angles the scattering is largely nuclear whereas at small angles it is more evenly divided between the electronic and nuclear scattering.

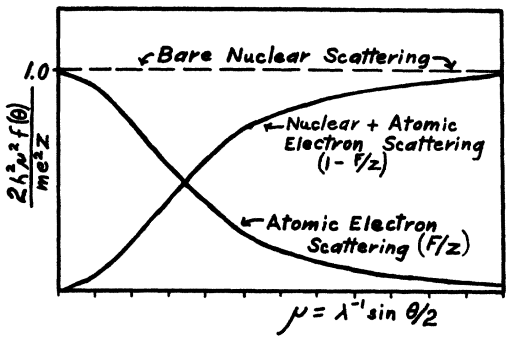

FIG. 8. Ratio of amplitude of wave scattered by atomic electrons and bare nucleus to that scattered by bare nucleus as a function of μ. See Eq. (29).

9. Scattering with Electron Exchange

In the two previous scattering theories one sought a solution of the stationary Schrodinger equation for the coupled system of atom and electron which represented an incident and a scattered wave. In these treatments the atomic electrons did not participate in the scattering event except insofar as they contributed to the potential field $V(r)$ of the scattering atom. When, however, the ψ of Schrödinger's equations is written so as to include the wave function of the bound as well as the scattered electron, there appears in the solution an effect which changes the predicted scattering curves considerably, especially for slow electrons. This effect, if it had a counterpart in the particle theory, would be that arising from the interchange of the colliding electron and the atomic electron at the moment of collision. The exchange of electrons requires a wave amplitude function ψ for the ejected electrons in addition to that required for those which are simply scattered without an exchange. The general theory of electron exchange was first developed by Oppenheimer[10] and later extended by Feenberg,[11] and Massey and Mohr.[12]

To illustrate the application of the theory of electron exchange to the problem of scattering, the relatively simple case of scattering by atomic hydrogen will be considered. Let $\psi(r_2)$ designate the wave function belonging to the bound electrons and let $F(r_1)$ be that of the colliding electrons. In a similar manner let $G(r_2)$ be the

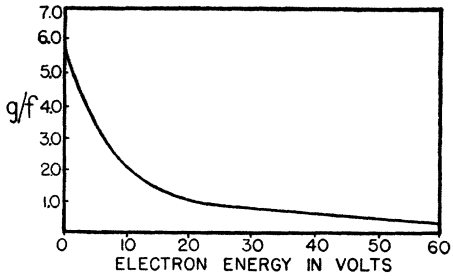

FIG. 9. Ratio of electron-exchange amplitude g to nonexchange amplitude f for scattering by hydrogen at 0°, Massey and Mohr, reference 12.

wave function representing the bound electrons which have been expelled and $X(r_1)$ be the wave function of those colliding electrons which replace those that are expelled. If the collision occurs without an exchange of electrons the wave equation is written as

$$(\nabla_1^2+\nabla_2^2+E+e^2/r_1 +e^2/r_2+e^2/r_{12})\psi_s(r_1, r_2)=0 \quad (31)$$

in which $\psi_s(r_1, r_2)$ may be expanded into

$$\psi_s(r_1, r_2)=\psi(r_2)F(r_1).$$

In the event of exchange the wave equation becomes

$$(\nabla_1^2+\nabla_2^2+E+e^2/r_1 +e^2/r_2+e^2/r_{12})\psi_e(r_1, r_2)=0 \quad (32)$$

in which $\psi_e(r_1, r_2)=G(r_2)X(r_1)$.

Just as before an asymptotic solution of the nonexchange Eq. (31) is desired which represents an incident and a scattered wave

$$F(r_1)=\exp(ikz)+f(\theta)r^{-1}\exp(ikr). \quad (33)$$

Also an asymptotic solution for the exchange Eq. (32) is sought, which has the form

$$G(r_2)=g(\theta)r^{-1}\exp(ikr). \quad (34)$$

If the electrons were distinguishable the number scattered would simply be proportional to f^2 and the number ejected proportional to g^2. The intensity of the scattered wave would then be

$$I(\theta)=|f+g|^2.$$

However, since the wave functions are required to be antisymmetric certain restrictions are placed upon the manner in which the amplitude of ejected electron wave and scattered electron wave combine. It can be shown[13] that the amplitudes so combine as to give the following intensity for the scattering wave

$$I(\theta)=\tfrac{3}{4}|f+g|^2+\tfrac{1}{4}|f-g|^2. \quad (35)$$

If the contribution from the ejected electron wave is small so that $g\to 0$, then the above expression again returns to the nonexchange solution, $I(\theta)=f^2(\theta)$.

Several approximate methods have been used to solve (31) and (32) and a fuller discussion will be deferred until later. The relative contribution from the g and f waves may be ascertained from the calculated f and g curves of Fig. 9. The contribution of the ejected electron wave g is illustrated here by plotting the ratio g/f as a function of the colliding electron energy. The data were calculated by Massey and Mohr for scattering in hydrogen at $\theta=0°$ by using a Born type of approximation to solve (31) and (32). It can be seen that the exchange process has the greatest effect upon the scattered wave at small electron velocities. In Fig. 10 Feenberg's scattering curves for helium as calculated with and without the exchange correction are also shown.

10. EARLY MEASUREMENTS

A method for studying electron scattering at one angle was devised by Hughes and Jones[14] (1926) and R. Kollath[15] (1928). Observations were made on the number of electrons scattered at the scattering angle of 90° while the energy of the colliding electron was varied. In effect these observers measured that fraction of the Ramsauer absorption coefficient which originated in the scattering of electrons at this one angle. A method which extended the observations to all angles was developed by Dymond[16] (1927). Dymond's observations over all angles were made possible by the introduction of a rotatable electron gun into the collision chamber. The gun

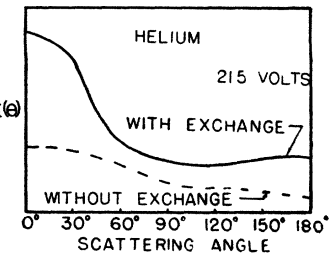

FIG. 10. Theoretical scattering curves, full line with exchange, dotted without exchange, Feenberg, reference 11.

was manipulated from the outside through a ground glass joint. The apparatus was similar to that shown in Fig. 11. Unfortunately in Dymond's first work the data were not reliable because of improper shielding in the collision chamber, as Harnwell[17] (1928) was able to show. Other scattering measurements made at this time were those by Dymond and Watson,[18] Harnwell,[19] Arnot,[20] McMillen[21] and Rose.[22] These experiments were carried out over the rather small angular range of 10° to 60° and over an electron energy range of from 8 to 200 electron volts.

In 1931 Bullard and Massey,[23] Arnot,[24] and Pearson and Arnquist[25] extended the angular range to 120° and made the interesting discovery that the scattering curves had a form suggestive of diffraction patterns. These were at once pointed to as new evidence for the wave-like behavior of electrons. It is interesting to note that the Faxen and Holtsmark[3] (1927) theory for electron scattering had been developed several years earlier and the data computed from which these diffraction curves could have been predicted. The theory and calculations were carried out for a comparison with experimental data on the closely related Ramsauer effect.

11. Measurement Methods

Scattering measurements are made by permitting a beam of electrons to penetrate a gas-filled chamber. This is illustrated in Fig. 11, where C is the gas-filled collision chamber and bb

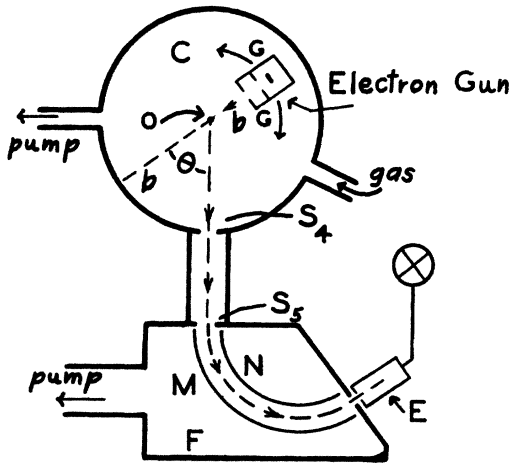

Fig. 11. Scattering apparatus with electron gun G, scattering chamber C, electron energy filter F and collector E; Hughes and McMillen, reference 32.

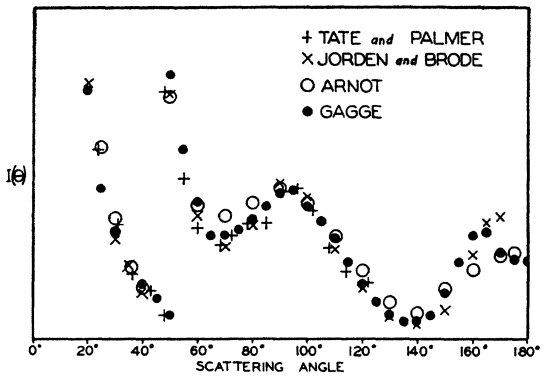

Fig. 12. Comparison of scattering measurements made by different observers on 80-volt electrons scattered in mercury.

the electron beam. Of those electrons that are scattered at the collision center O, some are scattered at a particular angle θ and enter the electron energy filter F. Here electrons of energies other than the desired one are filtered out of the scattered beam, those remaining pass on into the collector E. The collector is a sensitive current-registering device, such as an electrometer, which gives a measure of the number of electrons in the scattered beam. By rotating the gun G the magnitude of the scattered beam as a function of the angular gun setting or scattering angle is procured. The readings thus recorded are corrected to give the current of the scattered beam $I(\theta)$ per unit length of the collision path, per unit solid angle, per unit of initial electron beam current and per atom per unit volume. Measurements thus corrected are referred to as "scattering coefficients," "scattered intensity," or "effective cross section for scattering at the angle θ." Brode's[26] probability of scattering $S(\theta)$ is measured in terms of unit pressure at 0°C and is equal to $3.56\times10^{16}\ I(\theta)$.

The pressure in the collision chamber is kept low enough so that the probability of collecting electrons that have suffered more than one collision is negligibly small. This pressure is such that the electron m.f.p. is comparable with the dimensions of the collision chamber. The reproducibility of experimental scattering curves is indicated in Fig. 12, where the results of four observers[27–30] in four different laboratories are compared. The curves, as usual, have been fitted at some arbitrary point, since no absolute measurements were taken. In consideration of

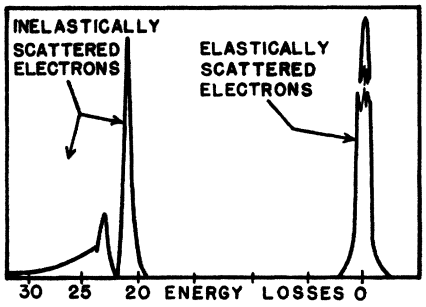

FIG. 13. Energy distribution of 50-volt electrons scattered at 10° in helium as determined by the electrostatic analyzer method, McMillen, reference 21.

the smallness of currents measured and the difficulties that are involved in the alignment of electron beam and receiving cone of the analyzer, the agreement is very satisfactory.

To measure the change of scattered intensity with energy of the colliding electrons is much more difficult, due to changes in the shape and orientation of the electron beam with electron energy. Also there is some doubt as to whether slits permit the passage of electrons equally well for all electron energies. An absolute determination of $I(\theta)$ requires such a precise knowledge of the effective geometry of the apparatus that it has been made by only one observer. Werner[31] constructed an apparatus especially designed to measure absolute scattering, and estimated his error of measurement to be as much as 10 percent for moderately fast electrons and 15–20 percent for 30- and 40-volt electrons.

The apparatus of Fig. 11 is that of Hughes and McMillen.[32] The electron gun is rotated about the collision center from the outside by means of a ground glass joint. The slit system S_4-S_5 defines the scattered beam and reduces the leak of gas into the filter. Potentials on M and N produce an electrostatic field which spreads the scattered electrons into groups according to their energies. The energy groups for 50-volt electrons scattered at 10° in helium is shown in Fig. 13. Because of the good resolution that is attained with the electrostatic analyzer, it lends itself readily to the study of inelastic scattering problems.

Arnot's[33] apparatus, shown in Fig. 14, differs from the above chiefly in the type of electron filter used. A retarding potential method is employed to repel charged particles other than elastically scattered electrons from the entrance to the collector. A potential on S_4 repels positive ions, and an appropriate one on S_5 repels inelastically scattered electrons. Since the resolution does not depend on the opening to the filter, as it does in the electrostatic analyzer, the method is particularly useful for measuring scattered currents of small intensity. A retarding potential analysis of a scattered beam for $\theta=7°$ in mercury is shown in Fig. 15. The curve is that obtained by Tate and Palmer[28] for 80-volt electrons. For this curve an apparatus similar to Fig. 14 was employed.

For slow electrons with energies below the excitation potentials no energy filter is necessary, and a simple collector like that of Ramsauer and Kollath,[34] shown in Fig. 16, suffices. It has the added advantage of possessing very large collecting areas which facilitate the measurement of scattered beams of small intensity. The collectors numbered 1 to 11 in the diagram are zones of a sphere which can be separately connected to an electrometer. The scattered current as recorded is proportional to the scattering between θ and $\theta+d\theta$ rather than per unit solid angle. The effective length of collision path and the average solid angle subtended by the zones are determined from the geometry of the apparatus. Ramsauer and Kollath were able to make observations with electrons of energy as low as 0.6 volt.

In the movable gun arrangement of Fig. 11 and Fig. 14 the small angle limit is set by the dimensions of the electron beam while the large angle limit is fixed by the width of the gun at the point where it intercepts the scattered beam. Gagge[30] surmounted the large angle limit difficulty by performing the experiment in the presence of a magnetic field which was aligned perpendicular to the scattering plane. Both the incident and scattered beams then have curved paths, and from Fig. 17 it is clear how for 180°

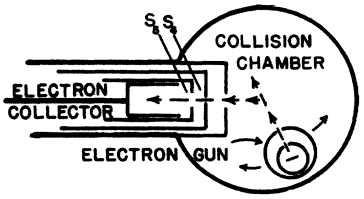

FIG. 14. Electron scattering apparatus utilizing a retarding potential method, Arnot, reference 33.

scattering the gun is in such a position as not to intercept the scattered beam. The gun in the 180° position is dotted in the diagram. The collector is mechanically moved from the outside so as to be in the proper position for collecting the elastically scattered electrons. The readings extended from 20° to 180°. In this method as well as in other methods the collector current readings are reduced to unit effective length of collision path. The variation of the correction near 180° is very much larger than the variation in the readings themselves, so that precise measurements on the geometry of the incident and scattered beams are very essential.

When the gas to be studied has an inappreciable vapor pressure at room temperature a special scattering chamber is required. Childs and Massey[35] constructed an apparatus in which the vapor was introduced into the collision chamber by means of a diffuse jet. The jet originates in the heated oven *O*, shown in Fig. 18, and condenses on a liquid-air trap *T*. Since in this case the collision volume is small the vapor density is approximately the same throughout the collision volume. A retarding potential method is used for energy analysis. Childs and Massey studied the scattering of cadmium and zinc with this apparatus. Since the effective pressure obtainable with the diffuse jet method is fairly small, McMillen[36] employed an apparatus in which the entire collision chamber was

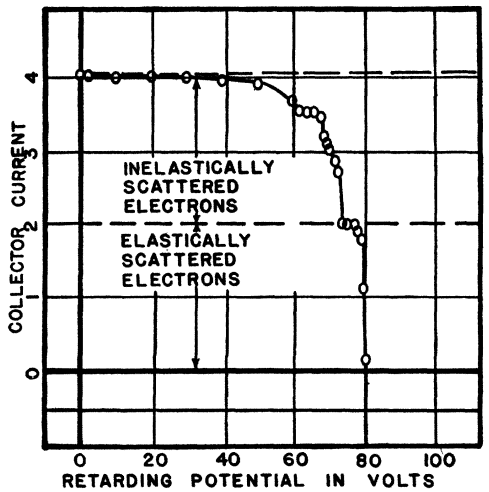

FIG. 15. Energy distribution of 80-volt electrons scattered at 10° in mercury as determined by the retarding potential method, Tate and Palmer, reference 28.

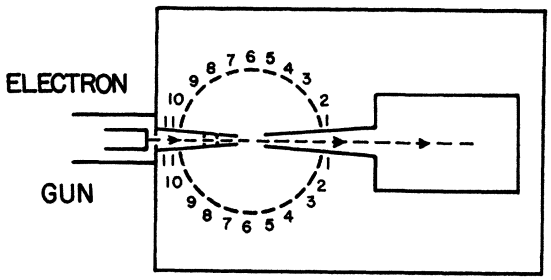

FIG. 16. Ramsauer and Kollath's (reference 34) scattering apparatus.

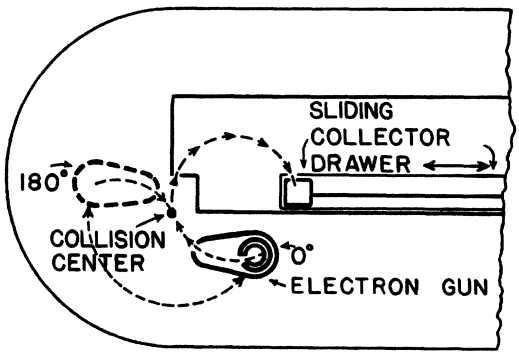

FIG. 17. Gagge's (reference 30) scattering apparatus with magnetic field perpendicular to diagram.

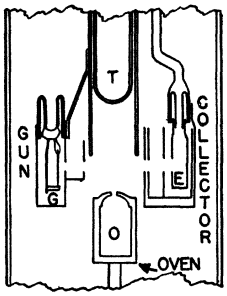

FIG. 18. Childs and Massey's (reference 35) scattering apparatus for vapors. Vapor from oven *O* condenses on liquid-air trap *T*. Electrons leave gun *G* and are collected at *E*.

kept at oven temperature. In this way the pressure maintained in the collision chamber was that corresponding to the oven temperature. The scattered beam intensity was quite large, and the apparatus yielded good results in a study of potassium.

12. SCOPE OF MEASUREMENTS

At present the scattering from twenty-five different gases has been observed. These include atoms whose atomic numbers range from $Z=1$ to $Z=80$. The angular range extends from about 5° to 180° and the observations have been made

with electrons whose energies extend from 0.6 to 2000 electron volts. A summary of the experimental data is given in Table I. The work of Kuper on helium, neon and argon might also be mentioned here even though the angular range of his measurements extended over the rather limited range of from 0.3° to 6.0°. The electron energies were large extending from 49,500 to 87,700 electron volts.

A typical scattering curve containing a diffraction pattern is shown in Fig. 19. The curves represent the scattering in mercury for various electron energies and were obtained by Arnot. When the scattered intensity $I(\theta)$ is plotted in polar coordinates the results are as shown in Fig. 20. This illustration appears in a paper by Ramsauer and Kollath[33] and concerns the scattering of slow electrons in argon.

13. Scattering in the Atomic Field Predominated by the Nucleus

The atomic field close to the nucleus is furnished almost entirely by the nucleus and the presence of the surrounding electrons may be safely disregarded. For small values of r the field $V(r)$ is purely a Coulomb field given by

$$V(r) = Ze^2/r.$$

Because the atomic field close to the nucleus is large, only the fastest electrons have a chance of reaching this region, and this they can do only if their impact parameter is small. Since all electrons with small impact parameters are scattered at large angles, one looks for evidence of nuclear scattering at large angles of scattering and in the scattering curves of fast electrons. The relationship between impact parameter, electron energy and scattering angle is given in (1). The distribution of electrons scattered by a bare nucleus is one which shows a predominance

Table I. *Gases in which elastic electron scattering measurements have been made.*

He[34, 41, 42]	Cd[35]	Br_2[46]
Ne[33, 34, 38, 41, 43]	H_2[33, 37, 38, 39, 40, 41]	I_2[46]
A[32, 33, 34, 38, 44, 47]	N_2[33, 38, 41]	PH_3[38]
Kr[33, 34, 46]	CO[33, 34]	H_2S[38]
Xe[33, 40]	CO_2[33, 38]	C_2H_6[49]
Hg[24, 27, 28, 30, 48]	C_2H_2[49, 50]	CCl_4[46, 52]
K[36]	CH_4[33, 38, 50]	$CHBr_2$[46]
Zn[45]	C_2H_4[49, 50]	CF_4[52]
		CBr_4[52]

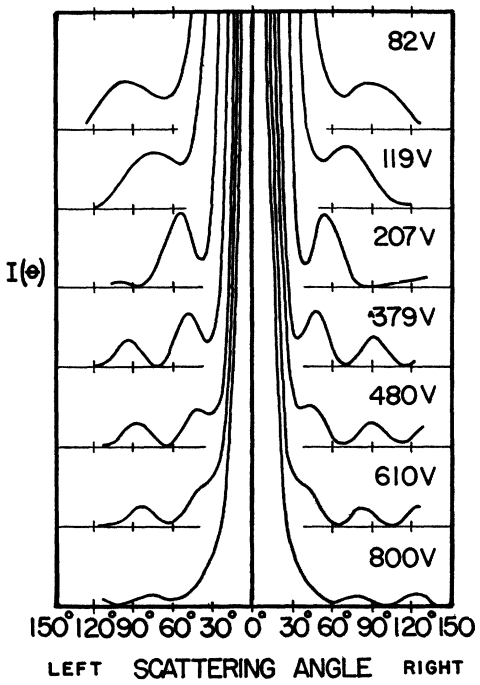

Fig. 19. Scattering curves for mercury, Arnot, reference 24.

of scattering in the forward direction. The scattering curve, according to (2), falls off monotonically with the scattering angle. The shape or the slope of the curve is the same for all nuclei and all electron energies, being independent of both Z and E.

An identical expression for nuclear scattering may also be obtained from the Born-Mott wave theory expression for atomic scattering. If in expression (30) the terms representing the contribution made by the atomic electrons are set equal to zero the expression then represents the intensity of the scattered nuclear wave and is identical with (2). It is also to be noted that the atomic electron terms in (30) go to zero when the atomic structure factor F goes to zero. This, as can be seen in Fig. 8, occurs for fast electrons and at large angles of scattering.

Experimental evidence of bare nuclear scattering is found in the scattering of 500-volt electrons by helium for scattering angles greater than 70°. The data obtained by Hughes, McMillen and Webb[42] are shown in Fig. 21, along with a curve calculated from the nuclear scattering expression (2).

Since the orbit followed by an electron is

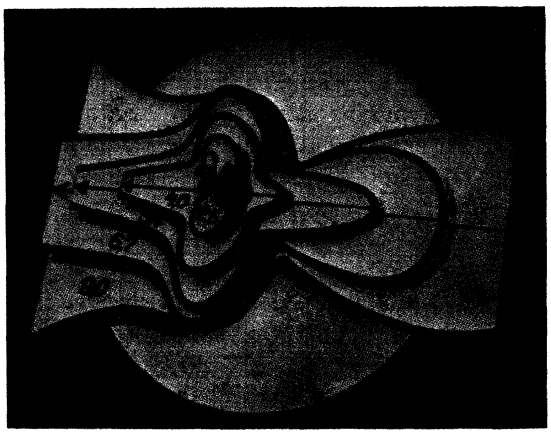

FIG. 20. Model of angular distribution of scattered electrons when plotted in polar coordinates, Ramsauer and Kollath, reference 34. Scattering gas is argon.

known whenever scattering by a bare nucleus takes place, it is possible to find how far into the atom these electrons penetrate. The particle theory gives for the distance of closest approach the expression

$$r_{\min}=\frac{2Ep^2}{Ze^2+(Z^2e^4+4E^2p^2)^{\frac{1}{2}}} \tag{36}$$

and for the impact parameter Eq. (1). For 500-volt electrons scattered at 90° by a helium atom one finds by using (1) and (36) that $r_{\min}=0.015$ angstrom. This is, as expected, well inside the atomic electron shell whose mean radius is about 0.3 angstrom.

An alternative experimental test for inverse-square law scattering is furnished by a measurement of the change in intensity of the scattered beam at a fixed scattering angle for varying electron energies. The intensity will, according to (2), vary inversely as the square of the electron energy. Werner[53, 54] carried out such an experiment, by collecting electrons scattered at 90°. Fig. 22 shows the apparatus. The collector is a

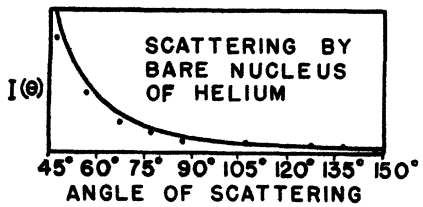

FIG. 21. Bare nucleus scattering in helium, 500-volt electrons. Full line, calculated; dots, experimental; Hughes, McMillen and Webb, reference 42.

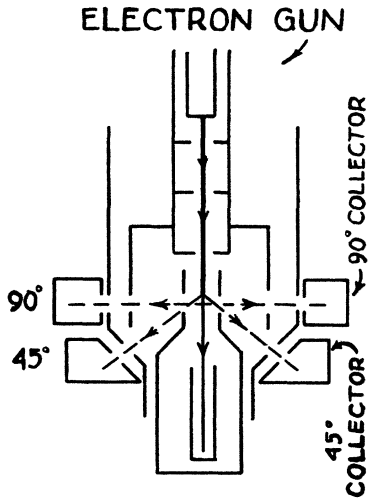

FIG. 22. Werner's (reference 54) apparatus for measuring the intensity of the scattered beam at two fixed angles, 45° and 90°.

hollow ring in a plane perpendicular to the electron beam. Electrons other than those elastically scattered were kept from the collector by

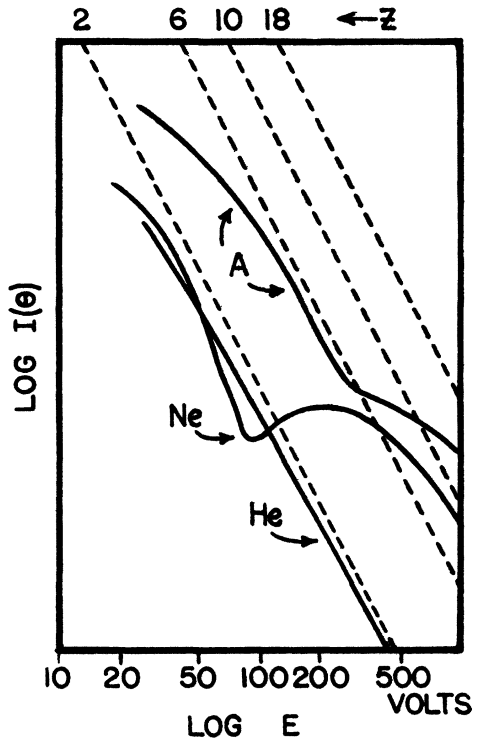

FIG. 23. Dotted lines show curves to be expected from scattering by bare nucleus. Full lines are Werner's (reference 53) observed values showing tendency to follow inverse-square law scattering for central charge corresponding to a shielded nucleus.

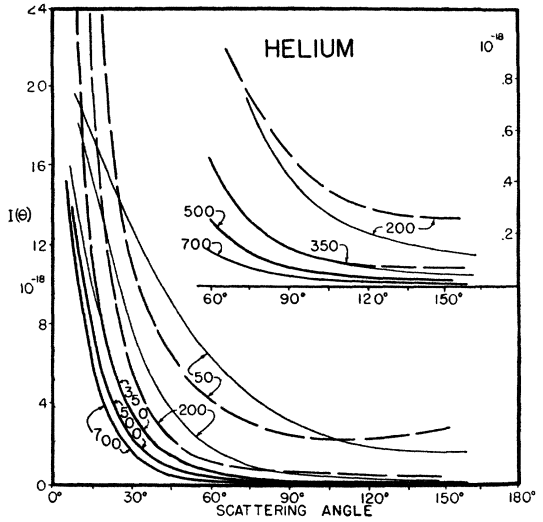

FIG. 24. Experimental scattering curves of helium (heavy lines) showing agreement with Born's theoretical curves (light lines) for fast electrons only. Hughes, McMillen and Webb, reference 42.

retarding potentials. Absolute measurements were made and the log of the scattered intensity plotted against the log of the electron energy. In this manner of representation the curve, if the scattering is inverse-square law scattering, is a straight line with an intercept proportional to Z^2. From Fig. 23 it can be seen that for helium the inverse-square law scattering is approached for electrons of 500 volts energy, and that the effective charge Z is as it should be, just 2.

For neon there is some evidence of inverse-square law scattering, but over a very limited region, that is, from about 30 to 75 volts. The nuclear charge is 2 rather than 10, which shows that the effective scattering field lies partly outside the external electron shells of the atom. In argon inverse-square law scattering appears between 100- and 200-volt electron energies, and indicates a net charge of about 6. Thus scattering for a fixed angle and a small energy range can at times take on the characteristics of inverse-square law scattering, and when it does the nuclear charge is partially reduced by the shielding effect of the atomic electrons.

14. Experimental Evidence Supporting Born's Theory

By working with helium, Hughes, McMillen and Webb[42] were able to show not only that the scattering followed the Born law but also, by making observations with electrons of various energies, they were able to determine the limiting electron energies for which the Born formula held. Their experimental results, extending from 10° to 170°, and for electrons of energy 50 to 700 volts, are shown in Fig. 24, where they are also compared with the theoretical Born curves. The heavy lines are drawn through the experimental points and are dashed only where they do not coalesce with the theoretical curves. These are represented as light full lines. It should be emphasized that all the experimental curves are drawn to one scale and all the theoretical curves drawn to one scale. There was but one arbitrary adjustment, and that was the fitting of the experimental and the theoretical 700-volt curves. It is apparent that for electrons whose energies are 500 volts or greater the Born scattering curves are in excellent agreement with the experimental curves. For 350-volt electrons and less the calculated curves become increasingly unlike the experimental ones, and in all cases underestimate the scattered intensity at both very large and very small angles.

For heavier atoms the tests of Born's theory reveal that the theory is insufficiently accurate to show agreement with the experimental curves except over a limited angular range. In mercury, for example, Jordan[48] finds that 2000-volt electrons follow the Born formula from 10° to 40° Arnot[33] also found agreement for 800-volt electrons in Xe, A and Kr up to a 60° scattering angle. Kuper,[51] by using 78,000-volt electrons, discovered that Born's theoretical curves coalesced with his experimental curves from 0.3° to 3° for argon, 1° to 3° for neon but not over any part of the angular range of 0.2° to 3° for helium.

In Werner's investigation of the scattering at a fixed angle with the apparatus shown in Fig. 22, great care was exercised in measuring the length of the collision path and effective dimensions of the collector so that absolute measurements might be made. His results are shown in Fig. 25, where the log of the scattered intensity is plotted against the log of the incident electron energy. Curve A is the calculated nuclear scattering, curve B that given by Born's formula, and C the experimental curve. The estimated error is indi-

cated in the figure. One observes that the absolute scattering measurements are in good agreement with those calculated for the electrons scattered at 90° as long as the electron energies are greater than 150 volts. At 45° the estimated error is larger but the experimental curve for 150-volt electrons lies just within the estimated experimental error.

15. Born Scattering and Atomic Electron Distribution

Whenever it is known that Born's theory of scattering is valid, it is possible to determine atomic structure factors and the atomic electron densities, $\rho(r)$ from the experimental scattering data. Let I represent the experimentally determined scattering values and R that to be expected from the bare nucleus of the scattering atom considered. Then Born's formula (30) becomes

$$I/R=(1-F/Z)^2$$

and

$$F=Z-Z(I/R)^{\frac{1}{2}}.$$

By combining this with the defining Eq. (26)

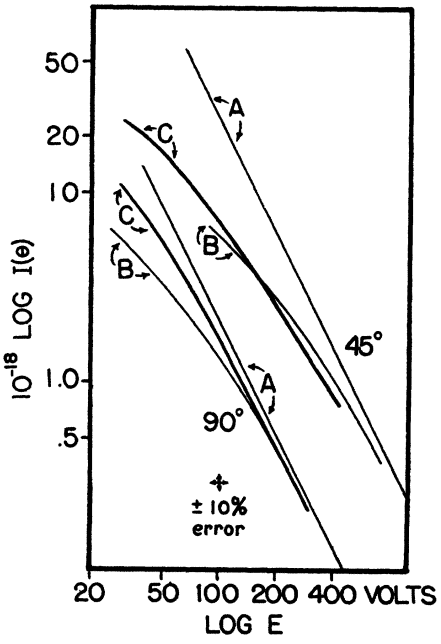

Fig. 25. Scattering at fixed angles in helium. Curve A, theoretical for bare nucleus; curve C, Born's theory; curve B experimental. No arbitrary adjustments on vertical scale. Werner, reference 31.

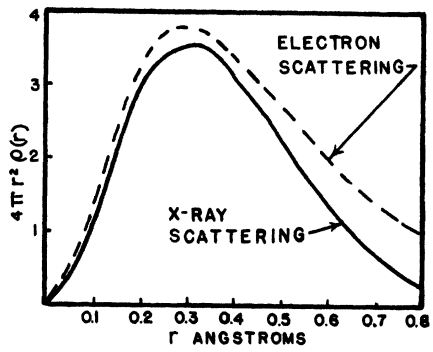

Fig. 26. Comparison of Morse's electron scattering determination of the electron density in helium with the x-ray scattering determination by Wollan.

for the atomic structure factor F we have

$$4\pi\int_0^\infty \rho(r)\frac{\sin(4\pi\mu r)}{4\pi\mu}rdr=Z-Z(I/R)^{\frac{1}{2}}. \quad (37)$$

Since both $\rho(r)$ and the right side of the above Eq. (37) may be expanded into a series of terms in sin $(4\pi\mu r)$, the above expression becomes, by Fourier's reciprocal theorem,[55]

$$4\pi r^2\rho(r)=r\int_0^\infty 4\pi\mu(Z-Z(I/R)^{\frac{1}{2}})$$

$$\times\sin(4\pi\mu r)d\mu. \quad (38)$$

Morse[56] used the above relationship to obtain the electron density distribution for helium. The experimental data I were taken from McMillen's observations on helium. Although these measurements included only small angles of scattering, Morse's calculated electron density curve agrees well with that found by Wollan from x-ray measurements. This is shown in Fig. 26, where Morse's and Wollan's electron densities are plotted against r.

16. Distorted Waves and Diffraction Patterns

In an earlier section it was pointed out that whenever the wave-lengths of the colliding electrons are much larger than the effective radius of the atom the scattering is accompanied by an appreciable distortion of the wave as it passed through the scattering atom. The resulting scattering curves reveal peaks and valleys suggestive of optical diffraction patterns.

The theory discussed in Section 4 gave expression (14) for the amplitude of the scattered wave. Each nth term or nth harmonic of (14) has an angular distribution given by $P_n(\cos\theta)$. The magnitude of each harmonic depends upon the value of n through the term $(2n+1)$ and upon the phase shift η_n appearing in the terms $(\cos(2\eta_n)-1)$ and $\sin(2\eta_n)$.

One important feature of the scattering expression (15) is that although the η's vary regularly with n they appear in (15) in trigonometric functions. These introduce erratic changes in the η terms as n takes on its consecutive values. The factor $(\cos(2\eta_n)-1)$, for example, is a maximum whenever the η's are equal to odd multiples of $\pi/2$. Upon that occasion the factor attains a value of 2. For even multiples of $\pi/2$ the factors are zero. The second factor involving the phase shifts, $\sin(2\eta_n)$, has a maximum value of unity when η is equal to odd multiples of $\pi/2$ and a zero value for even multiples of $\pi/4$. Thus the harmonics whose η's are near odd multiples of $\pi/2$ are the predominating ones, while those whose phase shifts have values equal to even multiples of $\pi/2$ and $\pi/4$ disappear from the scattering expression.

This behavior of the harmonics as n takes on its integral values is illustrated in Fig. 27. The data are calculated for the real part of expression (14) and refer to 100-volt electrons scattered at 30° in potassium. The phase shift terms oscillate about zero up to $n=3$ and thereafter rapidly fall off to zero. The terms involving n alone increase steadily with n. The θ term, $P(\cos\theta)$, varies, at least in the range $\theta=30°$ to $\theta=150°$, sinusoidally with n, and has a period proportional to θ^{-1}. The behavior of the harmonics as a whole, obtained by multiplying together the three terms comprising the harmonics, is shown in the lower part of the figure. The expression after the first few irregular variations takes on the appearance of a damped oscillation.

That the period of the variation of $P_n(\cos\theta)$ is proportional to θ^{-1} explains why at small angles the scattering is always large. Here the period is so long that a complete period is not attained before the phase shift values die out and only the positive values of $P_n(\cos\theta)$ occur. These add up to yield a large scattering amplitude. But at large angles the period is small,

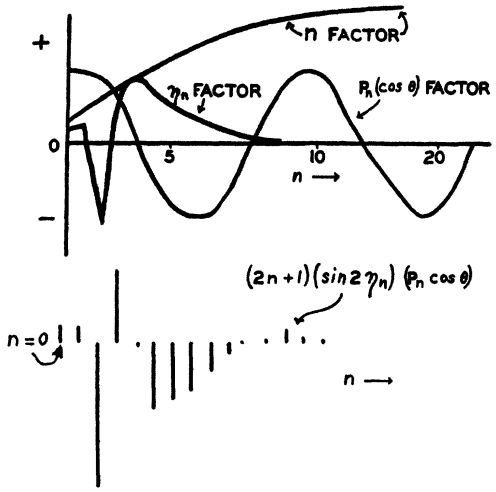

FIG. 27. Upper figure shows variation of $P_n(\cos\theta)$, phase shift factor and n factor belonging to real part of Eq. (14). Lower figure shows variation of real part of (14) as function of n. Scattering gas potassium, electron energy 100 electron volts, scattering angle 30°

promoting many oscillations, which when added together, because of their plus and minus values, yield a very small net amplitude.

17. Phase Shifts and Their Determination

The phase shift arises from a shift in phase of the radial component G, of the ψ wave as it passes through the atomic field $V(r)$. This component is a solution of the differential Eq. (10). The phase shift is measured with respect to the undeflected wave whose radial component g is a solution of (9). McDougall[5] has obtained the values for g and G for helium by solving (9) and (10). For $V(r)$ McDougall used the Hartree field data. His results are shown in Fig. 3. The full line is the shifted G_0 component and the dotted the g_0 component of the undeflected wave. One sees from the diagram that the magnitude of the shift decreases with increasing electron velocity. It is also clear that the range over which G is affected by the field increases for slow electrons.

A complete set of phase shift data for one atomic field is a set which gives values for all values of k as well as for all n values. Now since a set of phase shifts represents an atomic field, it should be possible, in theory at least, to determine these phase shifts from the experimental scattering curves and with these obtain

the atomic potential field $V(r)$. In practice, however, this is seldom carried out because the procedure is a lengthy one.

Exact method

The exact method is accomplished by the numerical integration of (10) with, of course, the proper boundary conditions. Holtsmark,[57] by following this rigorous but somewhat lengthy method, computed phase shifts for the atomic fields of argon and krypton. The field data employed by him were those of the Hartree field corrected for distortion of the atomic field by the electron, i.e., for polarization. McDougall also applied the exact method but used an unpolarized Hartree field. His phase shift data are for helium. A simplification in the numerical integration method which has greatly reduced the mechanical labor has been made by Hartree, Kronig and Petersen.[58] In their method all phase shifts are obtainable from a skeleton outline of initially calculated data. They furnish an extensive table of exact phase shifts for the atomic field of chlorine.

W-K-B-J method

Approximate methods of phase shift determinations, although less accurate, are frequently more desirable because of the ease with which the calculation can be carried out. A method due to Jeffreys yields expression (17). This solution is based on the assumption that R_a and R_p are separated by a finite interval and that the first integrand in the neighborhood of R_a and R_p behaves like r. For $n=0$ the latter assumption ceases to be true. However, in a similar method by Wentzel, Kramers,[60] and Brillouin, referred to as the W-K-B method, this assumption is more nearly valid. In this method, $n(n+1)$ in the above expression is replaced by $(n+\frac{1}{2})^2$. The two methods are identical for large n. Where it is convenient to refer to these two methods as one it is called the W-K-B-J method.

It is illuminating to examine the roots of the integrands of (17), namely R_a and R_p, for here one finds that if n is large they correspond to two famlliar quantities which occur in the particle theory of scattering. They are the distance of closest approach and the impact parameter p of an electron whose angular momentum is n and energy E.* Consequently we may say that the W-K-B-J method expresses the phase shifts as a function of that potential field existing between two specific radial distances, which on the particle theory are the closest distance of approach and the impact parameter. Thus one is able to associate the phase shifts with a specific region in the scattering field.

The usefulness of the W-K-B-J method was extended by Henneberg,[6] who incorporated the Thomas-Fermi field. Henneberg was able to show how, by a simple numerical process, phase shifts for one atomic number Z could be obtained from those of another atom of different atomic number Z'. By using Henneberg's relations one can obtain phase shifts for any atom whose atomic field can be accurately portrayed by the Thomas-Fermi field. Henneberg gives a fairly complete set of phase shifts for mercury.

Born method

A third method of computing phase shifts is the one given by Mott,[61] which is accurate only when the Born approximation is valid. If the exact scattering formula is equated to the Born expression one finds that the phase shifts are given by

$$\eta_n = \pi \int_0^\infty r V(r) (J_{n+\frac{1}{2}}(kr))^2 dr \qquad (39)$$

* To identify the roots of K_s in (18) when n is large, K_s is set equal to zero. Then one obtains

$$k^2 + 8\pi^2 m V(r)/h - n^2/R_a^2 = 0.$$

The replacement of k and n by their equivalent expressions in (4) and (19) gives

$$E + V(r) - Ep^2/R_a^2 = 0.$$

The energy equation for an electron following a path in a central force field is given by

$$(\tfrac{1}{2})m\dot{r}^2 + (\tfrac{1}{2})mr^2\omega^2 + V(r) = E$$

in which ω is the angular velocity. At the distance of closest approach the velocity $\dot{r}$ is zero and r by definition is R_a. This gives for the energy equation

$$(\tfrac{1}{2})mR_a^2\omega^2 + V(r) = E.$$

From the law of the conservation of angular momentum we have that $(\frac{1}{2})mR_a^2\omega^2 = p^2E^2/R_a^2$ which when substituted in the above defining energy equation for R_a gives an equation identical with that obtained above from K_s. To find the roots of K_u in (18) we have that

$$k^2 - n(n+1)/R_p^2 = 0$$

and upon replacing n by the expression given in (19) one obtains at once $R_p = p$.

in which $J(kr)$ are Bessel's functions. Since the expression is good only where the Born approximation is valid, the method gives satisfactory results only for η's less than 0.5 radian.

Allis and Morse method

Allis and Morse[62] have developed a method of finding the η's that is particularly well suited for the simplified atomic field model which they use. This model consists of a nucleus of charge Ze surrounded by a spherical shell of charge $-Ze$ at r_0. The phase shifts turn out to be functions of two parameters, $x=kr_0$ and $\beta=(Zr_0/2)^{\frac{1}{2}}$. Both quantities have significant interpretations. The quantity x is the ratio of the circumference of the spherical shell to the de Broglie wavelength of the incident electrons, while β is the square root of the integral of the effective charge $rV(r)$ and is a measure of the scattering power of the atom. Phase shift data have been tabulated by Allis and Morse for various sized atoms denoted by x and for atoms of various effective charges β.

In order to test the accuracy of the various approximate methods for determining the phase shifts, Arnot and Baines[63] calculated a set of phase shift values in which various approximate methods of calculation were used. For these calculations one field was used throughout. They employed the Hartree field for krypton and their data for 54-volt electrons are shown in Table II. Arnot and Baines concluded that except for the phase shifts for which n was very small or very large, the Jeffrey's method gave satisfactory values. The breakdown of the J-W-K-B method for large n's is somewhat compensated for by the fact that it is just here that the Born approximation method becomes valid. One observes in Table II that for phase shifts of 0.5 radian or less the Born method gives very satisfactory results. The W-K-B-J method is more accurate for atoms of small atomic number. This is brought out in Table III, in which η_0 for several of the inert gases are compared with the corresponding exact determinations of η_0. In view of the large errors involved in the determination of η_0, Hughes and Bilinsky[64] devised an extrapolation method for determining the η_0's of any electron energy when η_0's are exactly known for just two electron energies.

TABLE II. *Calculated phase shifts for 54-volt electrons scattering in krypton.*

PHASE	EXACT DETERMINATION	JEFFREY'S APPROXIMATION	BORN'S APPROXIMATION
0	9.696	10.612	
1	7.452	7.710	
2	4.469	4.748	
3	1.238	1.410	0.779
4	0.445	0.557	0.414
5	0.143	0.190	0.144

TABLE III. *Calculated phase shifts for the inert gases ($n=0$; $k=0$).*

$k=0$	EXACT METHOD	W-K-B-J METHOD
Krypton	4π	$4\pi+2.74$
Argon	3π	$3\pi+1.04$
Neon	2π	$2\pi+0.852$
Helium	π	$\pi+0.180$

One may summarize the effectiveness of the approximate methods by pointing out, as did Arnot and Baines, that in the calculation of phase shifts an exact method is advisable for the η_0's and the Born method for $\eta_n<0.5$. For all others the W-K-B-J method is the most convenient and satisfactory.

In the method of Allis and Morse, where the simple atomic field model was used, the phase shifts obtained by them were in excellent agreement with the absorption coefficient data. It is

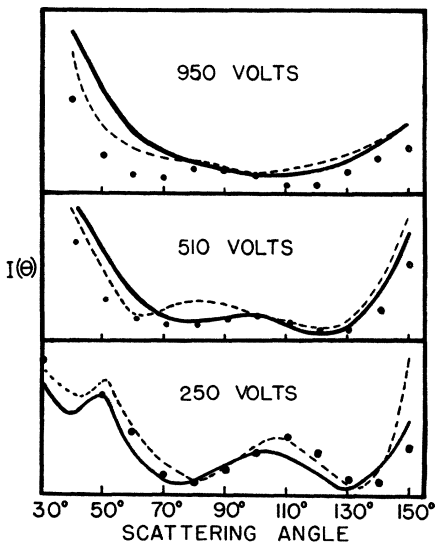

FIG. 28. Scattering curves of krypton calculated for Hartree fields, full lines, and for Thomas-Fermi fields, dotted lines. Experimental points, Webb, reference 64.

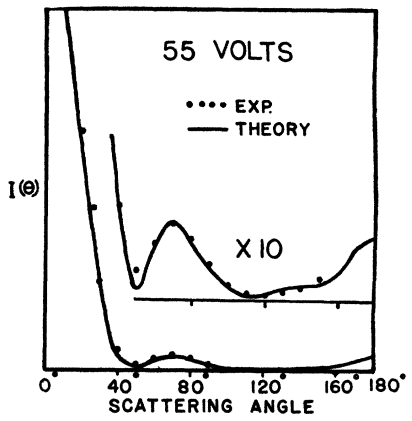

FIG. 29. Scattering curves for krypton calculated from a polarized Hartree field. Experimental points, Webb, reference 47.

somewhat surprising to find, then, that a very large difference exists in their phase shift values when they are compared with those obtained by a more accurate method. The differences are very large, especially for small n's. The application of these data by Allis and Morse to scattering curves of argon, however, showed that when electrons had energies between 16 and 40 volts there was fair agreement with the experimental curves. The data were not applied to scattering curves of other atoms, and it is difficult to estimate, in view of this lack of calculated data, to just what extent this simple model is successful in portraying the chief characteristics of the scattering curves.

18. Comparison with Existing Atomic Field Data

In comparing experimental data for electron scattering with the best available theories, one recognizes that an additional factor must be considered before judging too critically any discrepancy between theory and experiment. This factor is the atomic field data $V(r)$ which occurs directly or indirectly in all the scattering formulas. It would be desirable, perhaps, to convert experimental readings into field data $V(r)$ so that a direct comparison might be made between these experimental values and the theoretical values of the atomic field, such as the Hartree or Thomas-Fermi values. Unfortunately such a conversion is mathematically difficult and it has consequently become the practice to calculate scattering curves based on some theoretical atomic field and compare it with the scattering curve found experimentally.

The Hartree fields

In general, scattering curves for these fields have shown good agreement with the experimental curves. A comparison of the curves for krypton are shown in Fig. 28. The full line is the theoretical curve, based on Hartree's value. The calculations were made by Hughes and Bilinsky,[64] with Jeffrey's method for calculating the phase shifts.

Polarized Hartree fields

For slow electrons the scattering curves are much more susceptible to a polarized atomic field. Holtsmark[57] found that the Hartree fields gave theoretical absorption coefficients which agreed with the experimental measurements if the fields were corrected by the addition of a polarization term. The scattering curves for krypton based on the Hartree field which was corrected for polarization are shown in Fig. 29, where they are compared with the experimental curves of Webb.[47] Bullard and Massey[41] also found that the Hartree fields corrected for polarization were successful in fitting the experimental points of slow electron scattering in argon.

Thomas-Fermi field

That the Thomas-Fermi field should yield theoretical scattering curves which are not so good as those of the Hartree field is to be expected. A comparison of curves from these two fields is available in Fig. 28. The dashed curve is that computed with the Thomas-Fermi field. The phase shifts were calculated by Jeffrey's method. Although the general form of the experimental curve is evident in the theoretical curve obtained with the Thomas-Fermi field, the fit is somewhat better when the Hartree fields are used. Other tests of the Thomas-Fermi field were made with the Henneberg[6] phase shifts. These include 135- to 180-volt electrons in mercury,[6] 5- to 100-volt electrons in potassium,[36] and 80-volt electrons in argon. The curves for mercury are shown in Fig. 30. The Thomas-Fermi field is quite successful in presenting the principal features of the experimental curves and has

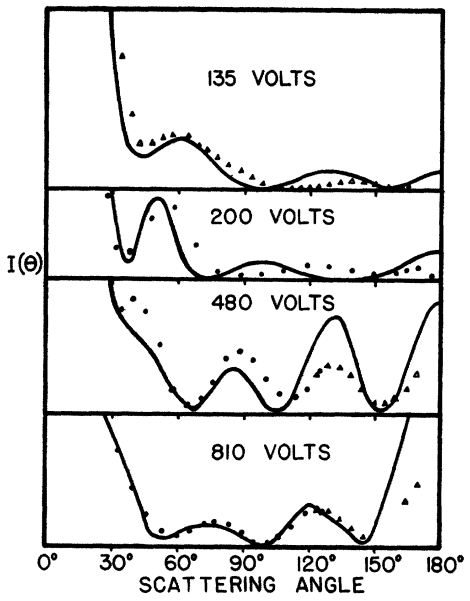

FIG. 30. Scattering curves for mercury calculated by utilizing the Thomas-Fermi field; Henneberg, reference 6. Experimental points; Arnot, reference 27 and Jordan, reference 48.

yielded curves that compare favorably with the measured curves for atoms of atomic number as low as 18.

Childs and Massey[45] find that for zinc the Thomas-Fermi field is inaccurate at large radial distances. As a substitute they employed a modified Thomas-Fermi field. For $r<r_0$ where r_0 is the radius of the M shell given by Slater's rules, the Thomas-Fermi values for $V(r)$ were used. For $r>r_0$ the field was extrapolated to give a zero value at the radius of the outer shell, which for zinc turned out to be at $r_0=2.1$ angstroms. With this field phase shifts were calculated by the W-K-B-J method. The computed curves gave good agreement with their experimentally obtained curves. The comparison was carried out for 30, 54 and 122-volt electrons.

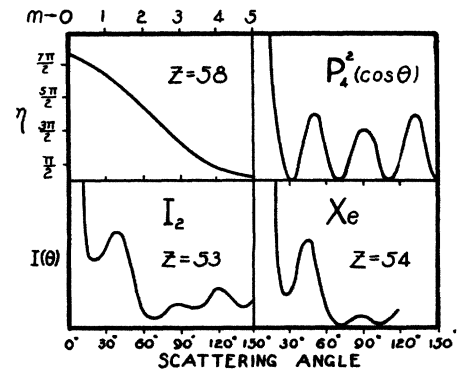

FIG. 31. Comparison of $P_4^2(\cos\theta)$ and experimental scattering curves of I_2 and Xe, also phase shift data for $Z=58$. Electron energies were 80 electron volts.

Successful as these correlations of theory and experiment have been, it is to be noted that for slow electrons scattering in helium and hydrogen the theory fails to give results which agree with the experimentally observed curves. This disagreement is caused, in part at least, by the failure to consider the effect of exchange as discussed in Section 9.

19. Diffraction Patterns and Atomic Number

The manner in which diffraction patterns vary with atomic number depends in part upon the energy of the electrons that are employed. We will at first confine ourselves to those electrons scattered just inside the valence electron shell, i.e., for electrons of energy just greater than that of the atomic ionization potential. An examination of these experimentally observed diffraction patterns reveals, first of all, that each one has a recognizable form and moreover, that these forms are identifiable in terms of Legendre coefficients. The following groups are easily recognized:

The P_4P_4 group

We observe that of the atoms of large Z there are two whose scattering curves show similar characteristics. These are I_2 and Xe. Their diffraction patterns are shown in Fig. 31 and contain three peaks located at 50°, 90° and 120° with valleys at 30°, 70°, 110° and 150°. The reason these are called the P_4P_4 group is apparent from an examination of the plot of $P_4^2(\cos\theta)$, which is also shown in the figure. It, too, exhibits three peaks located at 50°, 90° and 120°. The fact that the height of the experimental peaks is not the same as that given by the $P_4^2(\cos\theta)$ is obviously due to the other Legendre coefficients. These two elements, I of $Z=53$, and Xe of $Z=54$, include all the elements so far studied above $Z=48$, except mercury, which will be discussed later in conjunction with cadmium. The phase shift curve is also given in the figure and is presented as a function of n.

These data were obtained by interpolating between those for mercury and those for krypton, and thus the curve represents the phase shifts of an atom of atomic number $Z=58$.

The P_3P_3 group

The experimental scattering curves of Zn, Br_2 and Kr have two peaks and are classed as the P_3P_3 group. They resemble the function $P_3^2(\cos\theta)$ in that they show peaks at 60° and 120° and valleys at 40°, 90° and 130°. The experimental curves and $P_3^2(\cos\theta)$ are shown in Fig. 32. It will be noted that zinc with $Z=30$ tends to show some of the characteristics of the next lowest group, P_2P_2. These three atoms represent all that have been studied in the region $Z=30$ to $Z=48$. (Measurements made in cadmium $Z=48$ do not include electrons with energies as high as 80 volts.) The phase shift curve in the figure is that of krypton.

The P_2P_2 group

The gases PH_3, H_2S, A and K all have scattering curves showing a single peak. This is located at 90°. The experimental curves are shown in Fig. 33 with a plot of the function $P_2^2(\cos\theta)$ for purposes of comparison. Since the scattered intensity is roughly proportional to Z^2, the atoms in the molecules PH_3 and H_2S which play the important part in determining the nature of the scattering curves are the heavier ones, P and S. Consequently these scattering curves may for our purposes be regarded as atomic scattering curves. That the experimental curves are of the P_2P_2 type is self-evident. In the phosphorus curve $Z=15$, one notes that the 90° peak has almost disappeared. This is not surprising, in view of the fact that phosphorus is only five atomic numbers removed from neon. Neon's pattern is of the P_1P_1 type and has a valley at 90°. Chlorine, not shown in the diagram, also belongs to the P_2P_2 group. Its scattering curve is obtainable from measurements on CCl_4. The phase shift variation with n, also shown in the figure, was calculated from the Thomas-Fermi field of potassium.

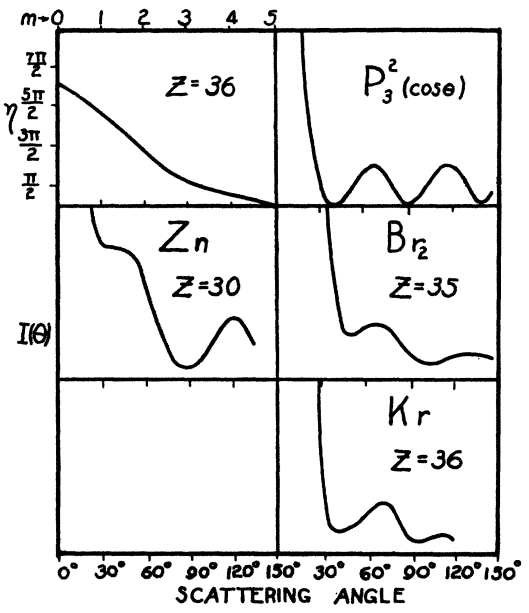

FIG. 32. Comparison of $P_3^2(\cos\theta)$ and experimental scattering curves of Zn, Br_2 and Kr, also phase shift data for $Z=36$; eighty-volt electrons.

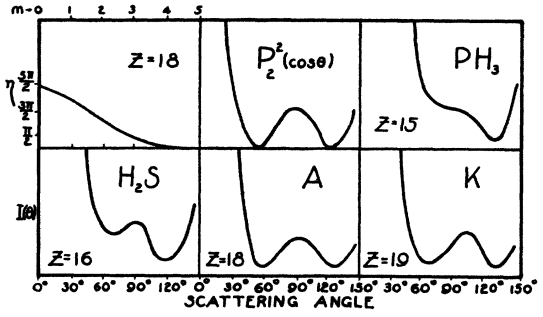

FIG. 33. Comparison of $P_2^2(\cos\theta)$ and experimental scattering curves of PH_3, H_2S, A and K, also phase shift data for $Z=18$; eighty-volt electrons.

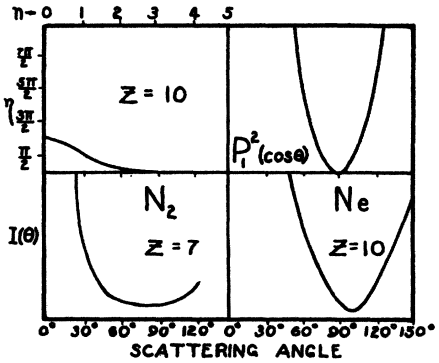

FIG. 34. Comparison of $P_1^2(\cos\theta)$ and experimental scattering curves of N_2 and Ne, also phase shift data for $Z=10$; eighty-volt electrons.

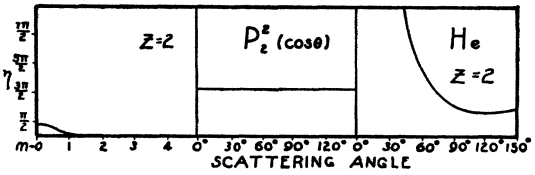

FIG. 35. Comparison of $P_0^2(\cos\theta)$ and experimental scattering curve for He, also phase shift data for $Z=2$; eighty-volt electrons.

The P_1P_1 group

This group includes N, Ne and possibly C. The scattering curves show a deep valley at 90° and can be represented by $\cos^2(\theta/2)$ which is $P_1^2(\cos\theta)$. These curves are shown in Fig. 34. The phase shift curve is for neon and is only approximately correct in that it was obtained by interpolating between the one for helium and the one for argon.

The P_0P_0 group

For helium and possibly carbon the experimental curves are rather flat and suggest a large contribution from $P_0^2(\cos\theta)$. See Fig. 35. Although the predicted diffraction curve for helium is flat, the effect of exchange, which was discussed in Section 9, give the curves a larger variation with angle. The phase shift curve is that calculated by McDougall for helium.

An explanation for these pattern types and their variation with Z is at once forthcoming from an inspection of the phase shift data. We shall for the most part follow the analysis originally made by Arnot.[46] One begins by recognizing that Born's scattering formula and the Faxen and Holtsmark expression (14) are equivalent over a certain narrow range of electron energies. Over this range Born's theory is exact and the incident wave is inappreciably distorted. It can be shown that the associated phase shifts in this range are small, never exceeding one-half radian. Let η_n' be those phase shifts which satisfy Born's requirements and are equal to or less than 0.5 radian. Then since $\exp(2i\eta_n')=(1+2i\eta_n')$ the expression for the amplitude of the scattered wave is

$$B^{\frac{1}{2}}=\frac{1}{2ik}\sum(2n+1)(2i\eta_n')P_n(\cos\theta) \qquad (40)$$

and the intensity for Born scattering becomes

$$B=\frac{1}{4k}(\sum(2n+1)(2i\eta_n')P_n(\cos\theta))^2$$

$$=\frac{me^4}{4h^4\mu^4}\left(1-\frac{F}{Z}\right)^2. \qquad (41)$$

If, however, only part of the amplitude harmonics have phase shifts satisfying the condition $\eta_n<0.5$, then the amplitude of the scattered wave may be written as the sum of those harmonics with $\eta_n'<0.5$ and those with $\eta_n>0.5$. Thus the amplitude is given by

$$I^{\frac{1}{2}}=B^{\frac{1}{2}}+\frac{1}{2ik}\sum_{n=0}^{n=\infty}(2n+1)\exp(2i\eta_n-1)$$

$$\times P_n(\cos\theta)-\frac{1}{2ik}\sum_{n=0}^{n=n'}(2n+1)$$

$$\times\exp(2i\eta_n'-1)P_n(\cos\theta) \qquad (42)$$

in which it is understood that n' is the index of the largest phase shift satisfying the requirements for Born scattering. Let η_n'' be the difference between the actual value of the phase shift and that required in Born's expression (40), that is, let $\eta_n''=\eta_n-\eta_n'$. Then (42) may be written

$$I^{\frac{1}{2}}=\frac{1}{2ik}\sum_{n=0}^{n=n'}(2n+1)\exp(2i\eta_n''-1)P_n(\cos\theta)$$

$$+\frac{1}{2ik}\sum_{n=0}^{n=n'}(2n+1)\exp(2i\eta_n'-1)P_n(\cos\theta)$$

$$+\frac{1}{2ik}\sum_{n=0}^{n=n}(2n+1)\exp(2i\eta_n'-1)P_n(\cos\theta) \qquad (43)$$

and

$$I=\left(B^{\frac{1}{2}}+\frac{1}{2ik}\sum_{n=0}^{n=n'}(2n+1)\exp(2i\eta_n''-1)\right)^2. \qquad (44)$$

If we neglect the cross products, which will be small, the expression for the scattered wave becomes

$$I=B+k^{-2}\sin^2\eta_0P_0^2(\cos\theta)$$
$$+9k^{-2}\sin^2\eta_1P_1^2(\cos\theta)$$
$$+25k^{-2}\sin^2\eta_2P_2^2(\cos\theta)+\cdots \qquad (45)$$

If the phase shifts for all n's are less than 0.5 radian, which is true incidentally for $Z=1$, all but the first term in (45) is zero and the scattering curve is simply a Born scattering curve which falls off monotonically with angle. As Z increases, the η's for each successive n attain values larger than 0.5 radian. The phase shift data in Figs. 31 to 35 show how as Z gets larger, one more η has a phase shift greater than 0.5. With each $\eta>0.5$ one more term in (45) is effective and the resulting scattering curves take on the following sequence of forms

$$\begin{aligned}
&\boldsymbol{B}\\
&B+\boldsymbol{P}_0\boldsymbol{P}_0\\
&B+P_0P_0+\boldsymbol{P}_1\boldsymbol{P}_1\\
&B+P_0P_0+P_1P_1+\boldsymbol{P}_2\boldsymbol{P}_2\\
&\cdot\quad\cdot\quad\cdot\quad\cdot\quad\cdot\\
&\cdot\quad\cdot\quad\cdot\quad\cdot\quad\cdot\quad\cdot
\end{aligned}$$

That this sequence of patterns is present in the experimental curves has already been noted. The pattern type, however, is that given solely by the Legendre coefficient of largest n. Arnot suggest that this may be due to the fact that phase shifts of lower n always have factors so nearly alike that the sum of their harmonics yield nothing but smooth curves. It may also happen, of course, that the phase shift angles for the lower n's consistently represent even multiples of $\pi/2$ which results in a cancellation of these phase shift factors. The Born scattering and background scattering from other Legendre coefficients is only prominent at the small angle region.

20. Diffraction Patterns for Heavy Atoms

That the phase shift data and scattering curves have changed in a regular manner with Z is to be taken as evidence that the atomic scattering field also varies in a regular manner with Z. A comparison, however, of the scattering curves for cadmium and mercury illustrates a situation in which the scattering curves do not depend upon Z in the manner found above. The diffraction patterns for both of these gases when electrons of 42 volts energy are used show identical characteristics, which at first seems very surprising in view of the great difference in their atomic numbers. Their scattering curves as obtained by Childs and Massey[35] are shown in Fig. 36. This apparent anomaly is explained away by Childs and Massey, who show that the electrons were scattered in that part of the atomic field which for these two atoms actually had the same magnitude and was located at the same radial distance from the center of the atom. They arrived at this conclusion from an inspection of the data shown in Table IV, which presents the main features of the outer shells of these two atoms. From the magnitude of the ionization potentials it is apparent that the electrons were scattered in the O shell of mercury and the N shell of cadmium. Since both the shell radii and ionization potentials are the same, the similarity in the scattering curves is understandable.

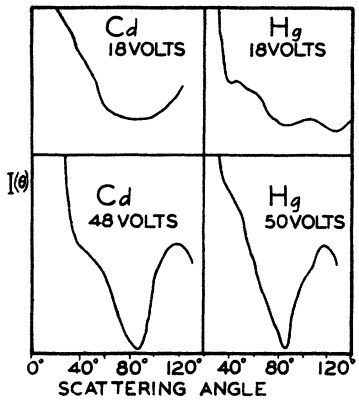

Fig. 36. Showing similarity in scattering curves of mercury and cadmium when scattered electrons have energies near 50 electron volts. Childs and Massey, reference 35.

Table IV. *Comparison of the atomic electron shells for* Hg *and* Cd.

Shell		Number of Electrons		Radius (in A)		Ionization Potential in Volts	
Hg	Cd	Hg	Cd	Hg	Cd	Hg	Cd
P	O	2	2	2.15	1.97	10.4	8.95
O	N	18	18	0.50	0.46	250	250
N	M	32	18	0.17	0.15	1800	1500

Table V.

Argon	Krypton	Mercury
$\boldsymbol{B}$	$\boldsymbol{B}$	$\boldsymbol{B}$
	·	·
$B+\boldsymbol{P}_0\boldsymbol{P}_0$	···	···
$B+P_0P_0+\boldsymbol{P}_1\boldsymbol{P}_1$	$B+\cdots\boldsymbol{P}_2\boldsymbol{P}_2$	$B+\cdots\boldsymbol{P}_3\boldsymbol{P}_3$
$B+P_0P_0+P_1P_1+\boldsymbol{P}_2\boldsymbol{P}_2$	$B+\cdots\boldsymbol{P}_2\boldsymbol{P}_2+\boldsymbol{P}_3\boldsymbol{P}_3$	$B+\cdots\boldsymbol{P}_3\boldsymbol{P}_3+\boldsymbol{P}_4\boldsymbol{P}_4$
$B+P_0P_0+\boldsymbol{P}_1\boldsymbol{P}_1$	$B+\cdots\boldsymbol{P}_2\boldsymbol{P}_2$	$B+\cdots\boldsymbol{P}_3\boldsymbol{P}_3$

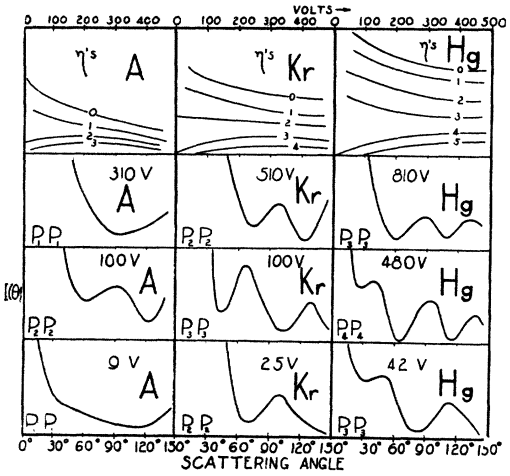

FIG. 37. Variation of diffraction patterns with energy of scattered electrons, and the associated phase shift curves.

Slower electrons such as 18-volt electrons are, however, influenced by the outer shell, which for these two atoms are not alike and hence give dissimilar scattering curves. The curves for 18-volt electrons are also shown in Fig. 36.

21. VARIATION OF DIFFRACTION PATTERNS WITH COLLIDING ELECTRON ENERGIES

A brief survey of the phase shift data for different electron energies show how the patterns change as electrons of different energies are considered. The very fastest electrons, those for which Born's approximation is valid, have η's less than 0.5 radian. These phase shifts increase for slower electrons and are roughly proportional to $(E)^{-\frac{1}{2}}$. As slower electrons are considered phase shifts are attained which are greater than the critical value 0.5 radian. These then manifest themselves in the scattering curves as additions to the Born scattering and reveal themselves in that angular range of the scattering curve at which the Born scattering is a minimum, namely at large angles.

Going to still lower electron energies, we find that not all phase shifts continue to increase. All those above and including a certain limiting η_n go to zero. This limiting η differs for different atoms; in mercury it is for $n=4$; in krypton $n=3$; in argon $n=2$, helium $n=1$. We show in Fig. 37 sketches of the phase shift data for mercury, krypton and argon. Because of this behavior of the η's for slow electrons, we may to a first approximation expect the patterns to take on the sequence of forms given in Table V as slower electrons are used.

B, as before, stands for Born scattering. Because certain of the η's approach zero as $E\rightarrow 0$ the predicted patterns go through a reversal. The patterns found experimentally follow Table V, except that they are all that of the type given by the largest n harmonic rather than a composite pattern of all the harmonics. This is the behavior also observed in Section 19. The experimental curves in Fig. 37 show this effect in argon. For slow electrons (310 volts) the curve is of the P_1P_1 type. Continuing to 100-volt electrons, the type becomes one of higher order P_2P_2, but reverts again to P_1P_1 for 9-volt electrons. For krypton, Fig. 37 shows the pattern going through the sequence $P_2P_2-P_3P_3-P_2P_2$. Mercury changes from P_3P_3 type to P_4P_4 and back again to P_3P_3. The patterns of the highest order are always for that n which is the first to go to zero as E approaches small values.

We continue our observation of the diffraction pattern variation with electron energy by considering what happens for very slow electrons, electrons for which the scattering takes place in the outer valence electron shells. Unfortunately sets of data for this class of electron energies are not very complete. Ramsauer and Kollath's[40] observation of the inert gases, hows ever, afford us at least one example of slow electron scattering. We show in Fig. 38 their curve-

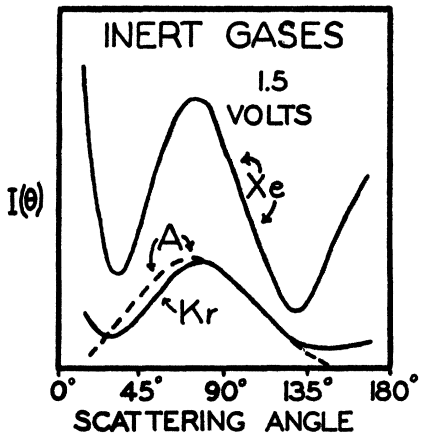

FIG. 38. Showing similarity of curves for the scattering of slow electrons in inert gases (reference 40).

for 1.5-volt electron scattering in argon, krypton and xenon. The curves all show the same pattern and thus betray those characteristics of the scattering field which pertain to the valence property of the atoms. We take these curves to be representative of slow electron scattering by closed shells.

22. Electron Exchange and Polarization Effects

For very slow electrons and scattering atoms such as helium and hydrogen the Faxen and Holtsmark theory even when incorporating the accurate Hartree fields, does not predict scattering curves that are entirely in agreement with experiment. This discrepancy has been shown to be due to two effects which become prominent for light atoms and scattered electrons of small energy. One of these is the exchange effect described in Section 9, the other an atomic polarization precipitated by the scattered electron. As shown in Fig. 10, the theoretical curves which have taken into account the effects of electron exchange show greater variation with angle than those which do not. Massey and Mohr's[12] exchange theory yeilds the curves shown in Fig. 39. In the same figure are shown the curves without exchange as calculated from the Faxen-Holtsmark's Eq. (15), in which Hartree fields were used. To show further that no reasonable change in the field will make the nonexchange curves more satisfactory, the scattering curves using the Allis and Morse field is also shown. One observes that only Massey and Mohr's electron exchange curves have the general form required by the experimental curves.

In the derivations of both the Born and

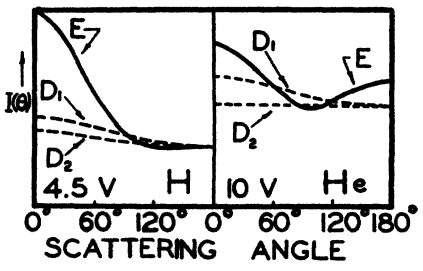

Fig. 39. E, theoretical scattering curves including electron exchange effects. D_2, theoretical curves using Hartree fields but no exchange effects. D_1, theoretical curves using Allis and Morse fields and no exchange effects.

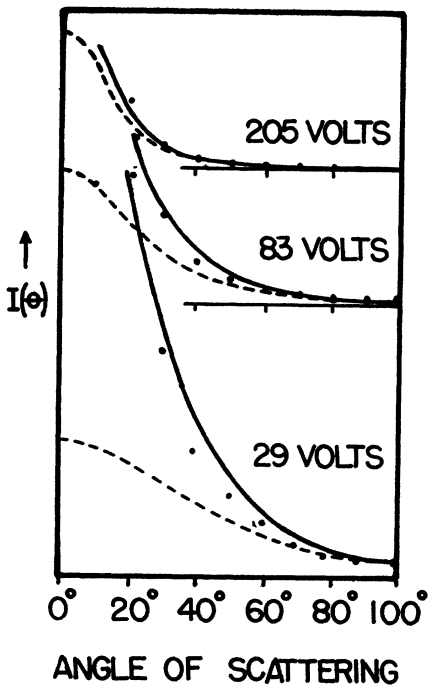

Fig. 40. Showing how experimental points for scattering in hydrogen follow Massey and Mohr's (reference 65) theoretical curves which include polarization effects. Full line, polarization; dotted line, without polarization.

Faxen-Holtsmark theories of scattering it was supposed that the atomic field was a static field and one not disturbed or polarized by the scattered electron. Actually this supposition is not entirely true, and atomic collisions when they occur with slow electrons are subject to a polarization effect. Holtsmark[57] showed, for example, that absorption coefficients for slow electrons could not be entirely accounted for if an unpolarized atomic field were used. Holtsmark, to meet the demands of the experimental absorption curves, was forced to add to the Hartree fields a term representing this effect. The polarization field which he chose fell off as r^{-4} at large distances from the center of the atom. The field after being corrected for polarization was later shown to give scattering curves that were in excellent accord with the observed curves. This is shown in Fig. 29.

Since the polarization field falls off as r^{-4}, the field becomes much larger than the field of the static atom at large distances from the atom. Thus a polarized atom, in contrast with the static atom, may be regarded as possessing an

additional spherical shell which is capable of scattering electrons and which lies outside the hitherto considered atomic boundary. Because the field is weak in this added shell, the electrons are deviated very little and the scattering curve shows an increase in the small angle scattering region.

Massey and Mohr[65] have shown that the polarization scattering may be expressed as the interaction of inelastically scattered electron waves and elastically scattered electron waves. They have obtained solutions for scattering in hydrogen and helium. Their scattering curves for hydrogen are shown in Fig. 40 and compared with the experimentally determined points. An interesting feature of Massey and Mohr's analysis is its prediction regarding the scattering at $\theta=0°$. Their solution reveals that for this angle the scattering becomes logarithmically infinite. All experimental evidence points to scattering in support of this since the curves rise rapidly at angles approaching $\theta=0°$.

23. Bibliography

1. Summaries of the theories of electron scattering appear in the following papers: E. U. Condon, Rev. Mod. Phys. **3**, 43 (1931); P. M. Morse, Rev. Mod. Phys. **4**, 577 (1932); and in the book: N. F. Mott and H. S. W. Massey, *Theory of Atomic Collisions* (Oxford Press, 1933).
2. N. F. Mott and H. S. W. Massey, reference 1, p. 91.
3. H. Faxen and J. Holtsmark, Zeits. f. Physik **45**, 307 (1927).
4. For a fuller account of this treatment, see N. F. Mott and H. S. W. Massey, reference 1, p. 19.
5. J. McDougall, Proc. Roy. Soc. **A136**, 549 (1932).
6. W. Henneberg, Zeits. f. Physik **83**, 555 (1933).
7. M. Born, Gott. Nach. p. 146 (1926); Zeits. f. Physik **38**, 803 (1926).
8. For details see N. F. Mott and H. S. W. Massey, reference 1, p. 87 or L. O. Brockway, Rev. Mod. Phys. **8**, 234 (1936).
9. N. F. Mott, Proc. Roy. Soc. **A127**, 658 (1930).
10. J. R. Oppenheimer, Phys. Rev. **32**, 361 (1928).
11. E. Feenberg, Phys. Rev. **40**, 40 (1932); **42**, 17 (1932).
12. H. S. W. Massey and C. B. O. Mohr, Proc. Roy. Soc. **A132**, 605 (1931); **A136**, 289 (1932).
13. N. F. Mott and H. S. W. Massey, reference 1, p. 74.
14. A. L. Hughes and L. W. Jones, Phys. Rev. **29**, 214 (1927).
15. R. Kollath, Ann. d. Physik **87**, 259 (1928).
16. E. G. Dymond, Phys. Rev. **29**, 433 (1927).
17. G. P. Harnwell, Proc. Nat. Acad. Sci. **14**, 564 (1928).
18. E. G. Dymond and E. E. Watson, Proc. Roy. Soc. **A122**, 571 (1929).
19. G. P. Harnwell, Phys. Rev. **34**, 661 (1929).
20. F. L. Arnot, Proc. Roy. Soc. **A129**, 361 (1930).
21. J. H. McMillen, Phys. Rev. **36**, 1034 (1930).
22. D. C. Rose, Can. J. Research **3**, 174 (1930).
23. E. C. Bullard and H. S. W. Massey, Proc. Roy. Soc. **A130**, 599 (1931).
24. F. L. Arnot, Proc. Roy. Soc. **A130**, 655 (1931).
25. J. M. Pearson and W. N. Arnquist, Phys. Rev. **37**, 970 (1931).
26. R. B. Brode, Rev. Mod. Phys. **5**, 258 (1933).
27. F. L. Arnot, Proc. Roy. Soc. **A140**, 334 (1933).
28. J. T. Tate and R. R. Palmer, Phys. Rev. **40**, 73 (1932).
29. E. B. Jordan and R. B. Brode, Phys. Rev. **43**, 112 (1933).
30. A. P. Gagge, Phys. Rev. **44**, 808 (1933).
31. S. Werner, Proc. Roy. Soc. **A139**, 113 (1933).
32. A. L. Hughes and J. H. McMillen, Phys. Rev. **39**, 585 (1932).
33. F. L. Arnot, Proc. Roy. Soc. **A133**, 615 (1931).
34. C. Ramsauer and R. Kollath, Ann. d. Physik **12**, 529 (1932); Physik. Zeits. **32**, 867 (1931).
35. E. C. Childs and H. S. W. Massey, Proc. Roy. Soc. **A141**, 473 (1933).
36. J. H. McMillen, Phys. Rev. **46**, 983 (1934).
37. G. M. Webb, Phys. Rev. **47**, 384 (1935).
38. C. B. O. Mohr, and F. H. Nicoll, Proc. Roy. Soc. **A138**, 469 (1932).
39. A. L. Hughes and J. H. McMillen, Phys. Rev. **41**, 39 (1932).
40. C. Ramsauer and R. Kollath, Ann. d. Physik **12**, 837 (1932).
41. E. C. Bullard and H. S. W. Massey, Proc. Roy. Soc. **A133**, 637 (1931).
42. A. L. Hughes, J. H. McMillen and G. M. Webb, Phys. Rev. **41**, 154 (1932).
43. A. L. Hughes and J. H. McMillen, Phys. Rev. **43**, 875 (1933).
44. F. H. Nicoll and C. B. O. Mohr, Proc. Roy. Soc. **A142**, 320 (1933).
45. E. C. Childs and H. S. W. Massey, Proc. Roy. Soc. **A142**, 509 (1933).
46. F. L. Arnot, Proc. Roy. Soc. **A144**, 360 (1934).
47. G. M. Webb, Phys. Rev. **47**, 379 (1935).
48. E. B. Jordan, Phys. Rev. **45**, 47 (1934).
49. E. C. Childs and A. H. Woodcock, Proc. Roy. Soc. **A146**, 199 (1934).
50. A. L. Hughes and J. H. McMillen, Phys. Rev. **44**, 876 (1933).
51. J. B. H. Kuper, Phys. Rev. **53**, 993 (1938).
52. S. Hill and A. H. Woodcock, Proc. Roy. Soc. **A155**, 331 (1936).
53. S. Werner, Nature **131**, 726 (1933).
54. S. Werner, Proc. Roy. Soc. **A134**, 202 (1931).
55. M. Muskat, Phys. Rev. **35**, 1583 (1930).
56. P. M. Morse, reference 1, p. 598.
57. J. Holtsmark, Zeits. f. Physik, **66**, 49 (1930).
58. D. R. Hartree, R. deL. Kronig and H. Petersen, Physica **1**, 901 (1934).
59. H. Jeffreys, Proc. London Math. Soc. (2), **23**, 428 (1923).
60. H. A. Kramers, Zeits. f. Physik **39**, 828 (1926).
61. N. F. Mott, Proc. Camb. Phil. Soc. **25**, 304 (1928).
62. W. P. Allis and P. M. Morse, Zeits. f. Physik **70**, 567 (1931).
63. F. L. Arnot and G. O. Baines, Proc. Roy. Soc. **A146** 651 (1934); F. L. Arnot, Proc. Camb. Phil. Soc. **32**, 161 (1936).
64. A. L. Hughes and S. Bilinsky, Phys. Rev. **48**, 155 (1935).
65. H. S. W. Massey and C. B. O. Mohr, Proc. Roy. Soc. **A146**, 880 (1934).

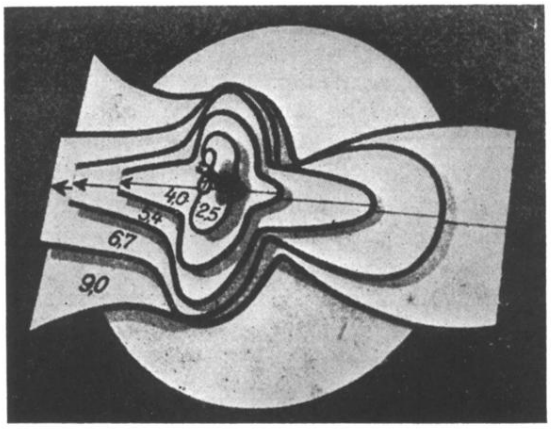

FIG. 20. Model of angular distribution of scattered electrons when plotted in polar coordinates, Ramsauer and Kollath, reference 34. Scattering gas is argon.